الجـــــــــــــــــــــمـهـوريـــــة الجـــــــــــــزائـريـة الديمـــــــقـراطيـة الـشـــــــــعبيـة

REPUBLIQUE ALGERIENNE DEMOCRATIQUE ET POPULAIRE

وزارة التـــــــــــــــــــــــــــــعـليـم العـــــــالي و البـــــــــحث العـــــلـمـــي

Ministère de l'Enseignement Supérieur et de la Recherche Scientifique

جـــــــــــــــامعة أبي بكـــر بـلـقـايد – تـلمســـــــــــــــان –

Université Aboubakr Belkaïd – Tlemcen –

Faculté de TECHNOLOGIE

MEMOIRE

Présenté pour l'obtention du **diplôme** de **MASTER**

En : Génie Mécanique

Spécialité : Construction Mécanique

Par : NHAMBURO Estroge Tinotenda

Sujet

Mesure de la température de coupe lors d'une opération de tournage orthogonale

Soutenu publiquement, le 09/ 06 /2024 , devant le jury composé de :

M : GHERNAOUT Mohamed El Amine	Professor	Univ. Tlemcen	Président
Mr. KARA ALI Djamal Abdelillah	MCA	Univ. Tlemcen	Encadreur
Mr. BENHADJI SERRADJ Nasr-eddine	MCB	ESSA Tlemcen	Co- Encadreur
M: BELALIA Ahmed	Professor	Univ. Tlemcen	Examinateur

Année universitaire 2023/2024

الجـــــــــــــــــــــــمهـوريـــــة الجـــــــــــــزائـريـة الديمـــــــقـراطيـة الـشـــــــــعبيـة

DEMOCRATIC AND POPULAR REPUBLIC OF ALGERIA

وزارة التـــــــــــــــــــــــــــــعليـم العـــــــالي و البـــــــــحث العـــــلـمـــي

Ministry of Higher Education and Scientific Research

جـــــــــــــــامعة أبي بكـــر بـلـقـايد – تـلمســـــــــــــــان –

Aboubakr Belkaïd University – Tlemcen –

Faculty of TECHNOLOGY

THESIS

Presented to obtain a **MASTER'S degree**

In : Mechanical Engineering

Specialty : Mechanical design

By : NHAMBURO Estroge Tinotenda

Topic

Measurement of cutting temperature during orthogonal turning

Defended publicly, on 09/06/ 2024 , before the jury composed of :

M : GHERNAOUT Mohamed El Amine	Professor	Univ. Tlemcen	President
Mr. KARA ALI Djamal Abdelillah	MCA	Univ. Tlemcen	Supervisor
Mr. BENHADJI SERRADJ Nasr-eddine	MCB	ESSA Tlemcen	Co- Supervisor
M: BELALIA Sidi Ahmed	Professor	Univ. Tlemcen	Examiner

Academic year 2023/2024

ACKNOWLEDGEMENTS

Firstly I would like to thank God for his guidance throughout the course of my work. I would also like to extend my gratitude to my supervisors, Dr KARA ALI Abdelillah Djamal and Dr BENHADJI SERRADJ Nasr-eddine for their unwavering guidance, insightful feedback, and patience. Their expertise and mentorship were invaluable, and I am grateful for the countless hours they spent reviewing my work.

I extend my gratitude to Mr GHERNAOUT Mohamed El Amine for presiding over the jury of my defense. I am also grateful to Mr BELALIA Ahmed for examining my work.

I would like to thank my family for standing by me during moments of doubt and celebrated my achievements. Their unwavering support sustained me throughout this process. To my friends, thank you for your encouragement and understanding. To my friends, your presence during late-night writing sessions brought comfort and motivation. In writing this thesis, I stand on the shoulders of these remarkable individuals. Their contributions, whether big or small, have left an indelible mark on my academic journey.

Last but not least, I would like to extend my gratitude to the Algerian and Zimbabwean governments for affording me this academic opportunity and all the resources I have been allowed access to during my academic journey.

Dedication

To God my heavenly father

To my father

To my siblings

To my friends

Abstract

During machining, heat is generated at the tool workpiece interface as a result of the energy generated during shear deformation of the workpiece. This heat is a function of cutting parameters used during machining and it affects the lifespan of the cutting tool and the quality of the machined surface.

The goal of this work is to measure the cutting temperature of the tool workpiece interface during orthogonal machining using an infrared camera. The experimentation performed in this work will contribute to the understanding of how different cutting parameters affect the temperature of orthogonal cutting.

The measurement of cutting temperature is recorded with a FLIR infrared camera mounted on a parallel lathe. The experimental design method was employed to find the number of experiments needed develop a mathematical model of temperature prediction.

Keywords: machining, workpiece, orthogonal machining, experimental design, infrared camera, lathe

Résumé

Pendant l'usinage, la chaleur est générée à l'interface de la pièce et l'outil en raison de l'énergie générée lors de la déformation par cisaillement de la pièce. Cette chaleur est fonction des paramètres de coupe utilisés lors de l'usinage et affecte la durée de vie de l'outil de coupe et la qualité de la surface usinée.

L'objectif de ce travail est de mesurer la température de coupe de l'interface de la pièce et l'outil lors de l'usinage orthogonal à l'aide d'une caméra infrarouge. L'expérimentation réalisée dans ce travail contribuera à la compréhension de la façon dont différents paramètres de coupe affectent la température de la coupe orthogonale.

La mesure de la température de coupe est enregistrée avec une caméra infrarouge FLIR montée sur un tour parallèle. La méthode de plan d'expérience a été utilisée pour déterminer le nombre d'expériences nécessaires pour développer un modèle mathématique de prédiction de la température.

Mots-clés : usinage, pièce, usinage orthogonal, plan d'experience, Caméra Infrarouge, tour

ملخص

أثناء التصنيع ، تتصاعد الحرارة اعند واجهة قطعة و الأداة نتيجة للطاقة المتولدة أثناء نزع المادة لقطعة. هذه ما يؤثر على عمر أداة القطع وجودة السطح التصنيع.

الهدف من هذا العمل هو قياس درجة حرارة الأداة اثناء عملية الخراطة باستخدام كاميرا الأشعة تحت الحمراء. ستساهم التجارب التي تم إجراؤها في هذا العمل في فهم كيفية تأثير عناصر القطع على درجة حرارة الأداة.

يتم تسجيل قياس درجة حرارة القطع باستخدام كاميرا FLIR تعمل بالأشعة تحت الحمراء مثبتة على مخرطة متوازية .تم استخدام تصميم التجربة لتطوير نموذج رياضي للتنبؤ بدرجات الحرارة.

الكلمات المفتاحية: شروط القطع ، التصوير الحراري، الشغل ، تصميم التجربة ،

Contents

List of figures

CHAPTER I: Overview of machining

CHAPTER 2: INFRARED CAMERA

CHAPTER 3: EXPERIMENTATION

CHAPTER 4: RESULTS AND DISCUSSION

List of Tables

CHAPTER I: Overview of machining

CHAPTER 3: INFRARED CAMERA

CHAPTER 4: RESULTS AND DISCUSSION

Nomenclature

N: rotation speed(tr/min)

Vc: cutting speed(m/min)

D: diameter(mm)

Q: duantity of removed material(mm^3/min)

p: depth of feed(mm)

***c*:** wave propagation speed(m/s)

λ: wavelength(m)

a: feed rate(mm/tr)

υ: frequency(Hz)

E: emissivity

R: reflectivity

T °: temperature(°C)

T_{exp}: experimental temperature(°C)

T_{pred} : predicted temperature(°C)

***e_i*:** error(%)

***A_i*:** precision(%)

IR: infrared camera

ANOVA: analysis of variance

n: number of experiments

Introduction

Every physical product that exists has gone through at least one manufacturing process. What we call manufacturing today has been part of our civilisation as far back in time as before recoded history. Manufacturing is an important part of the welfare of any society, for both technological and economic advancement. One of the most important manufacturing processes is conventional machining, which is part of a family called material removal processes.

Material removal processes involve the removal of excess material is removed from a workpiece to obtain a desired geometry. Perhaps the most important branch of material removal processes is conventional machining. During machining, a cutting tool with a specially designed cutting-edge causes shear deformation of the workpiece to form and remove a chip. Thus, exposing a newly formed surface.

The two main phenomena involved in this process are; shear deformation of the in the primary, secondary and tertiary shear zones, friction between the chip and the tool's rake face. Some of the energy generated in this process is converted into heat, which affects the manufactured surface and may cause failure of the cutting tool.

The measurement and surveillance of cutting temperature is an active field of research, several methods of temperature measurement and prediction during the machining process have been developed over the years. To contribute to the technological advancement in manufacturing domain, it is important to have methods of prediction of cutting temperature, and how different machining parameters affect the cutting temperature. This enables the development of new, more resilient materials for the manufacture of cutting tools and the optimization of the cutting process in general.

The main objective of this work is to measure the cutting temperature during orthogonal machining.

This work is divided into four chapters consisting of the following aspects:

The first chapter includes bibliographic research. It goes through an overview of the material removal process, mainly focusing on turning, including cutting conditions and a look at orthogonal cutting and how it differs from oblique cutting. Finally, the chapter covers the different methods of temperature measurement during machining.

The second chapter takes a look at the infrared camera and infrared thermography. It also describes thermal radiation and the notion of emissivity. Lastly the chapter describes some methods used for the calibration of infrared camera.

The third chapter is a presentation of the materials used in this study, description of the parallel lathe, band saw machine and the Flir 305Sc infrared camera including their characteristics. It also gives an overview of the camera software interface (Flir QuickPlot). The chapter concludes with experimental planning and presentation of tabulated experimental results.

The last chapter is dedicated to the discussion of experimental results. That include tracing curves and interpreting them.

Finally, we do an analysis and a synthesis of the results we obtained to come up with a conclusion for this work.

CHAPTER I: **Overview on turning**

I.1 Introduction

The removal of material requires the use of a physical element that extracts material from a basic volume (bar, block, plate, etc.) in order to obtain a finished or semi-finished part [1]. As shown in the figure below, there are several material removals processes that are currently used in the industry among them, conventional machining, abrasion machining, and unconventional machining.

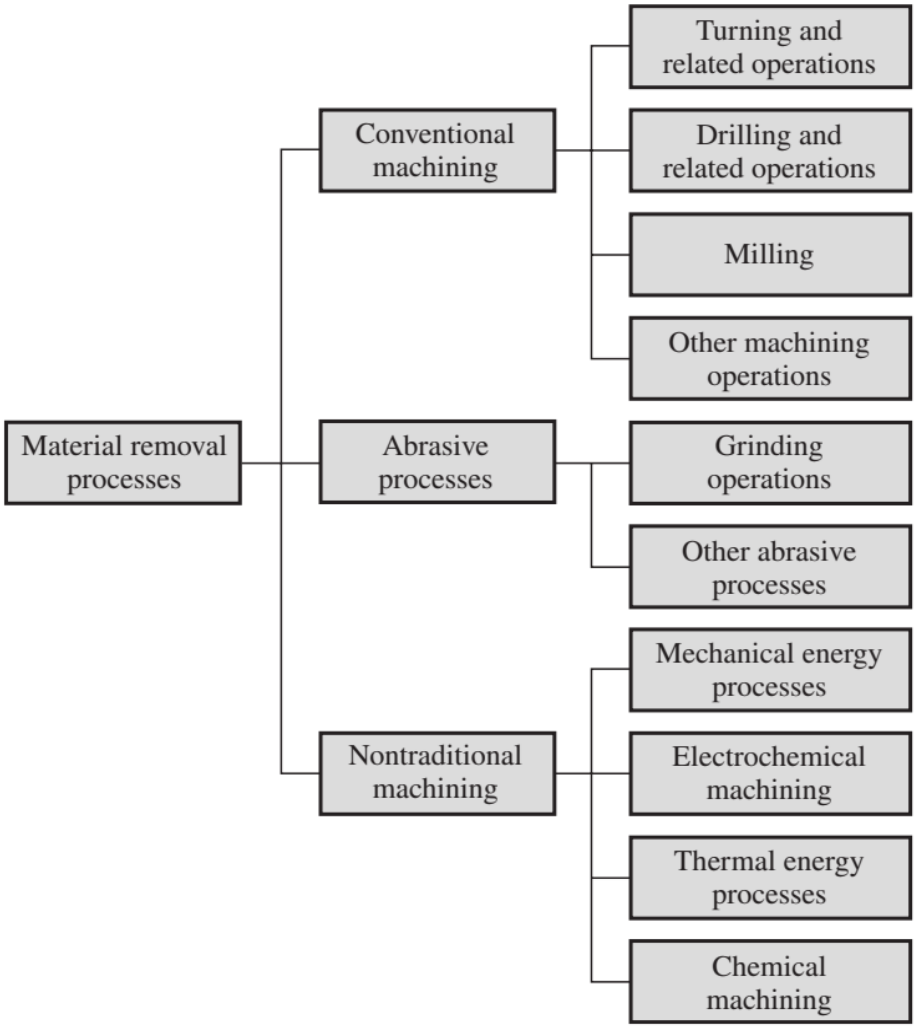

Fig. I.1: Classification of material removal processes. [4]

I.2 Turning

I.2.1 Definition

Turning is the machining process that made it possible to obtain round parts (cylindrical and/or conical in shape) using sharp tools on machines called lathes [1]. Turning is one of the processes of manufacturing mechanical parts by removing the material. The most important process is conventional machining, in which a sharp tool is used to cut material to achieve a well-defined geometry. [4] The main action in conventional machining is the shear deformation of the workpiece in order to produce chips that are removed by the sharp stop of the cutting tool. [4] For these types of operations, the tool and the workpiece must be in relative motion. Relative motion is given by two types of motion called cutting motion and forward motion [1]. In the shooting. The part is animated by a rotational movement (cutting movement), which is the main movement of the process. The tool is animated by a complementary translational movement called the feed movement, which allows the profile of the part to be defined [2]

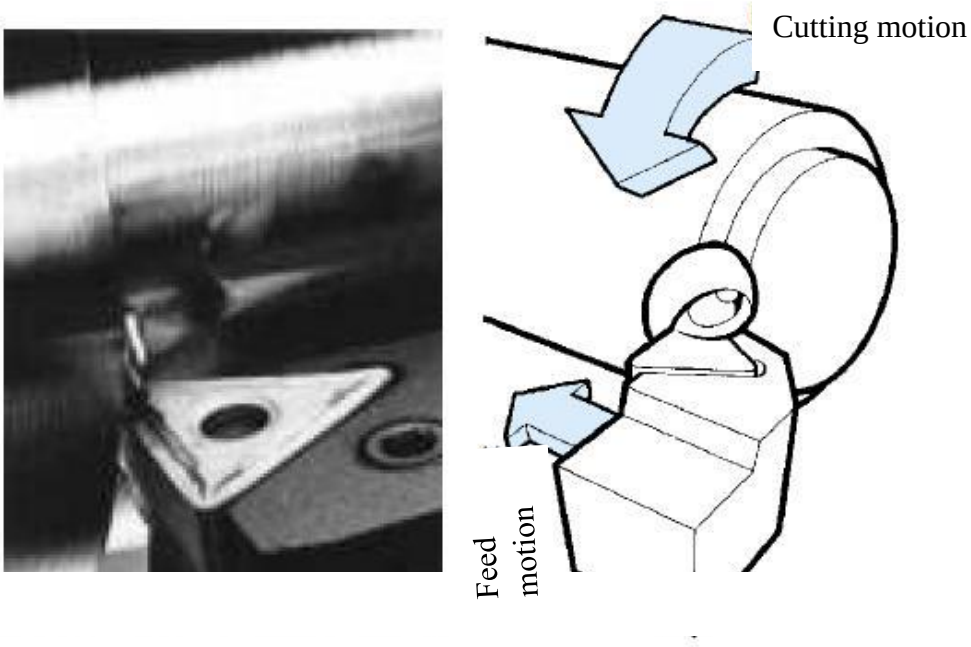

Fig. I.2: Illustration of cutting and feed motions. [39]

I.2.2 Cutting conditions

There are three important quantities in the production of parts by material removal. The primary movement is the cutting speed Vc or N (number of revolutions per minute). The relationship between Vc and N is given the following equation:

$$N = Vc \cdot 1000 / \pi \cdot D \quad \text{(tr/min)}$$

Where D is the diameter of the workpiece in mm.

The secondary motion is the feed motion ***a*** which is related to another quantity called the cutting depth ***a*** and the quantity of matter removed ***Q*** by the following formula:

$$Q = Vc.a.p \quad (mm^3/min)$$

Where ***Vc***: Cutting speed(m/min); ***a*** : feed rate(mm/tr) and ***p*** : depth of cutting(mm). [1]

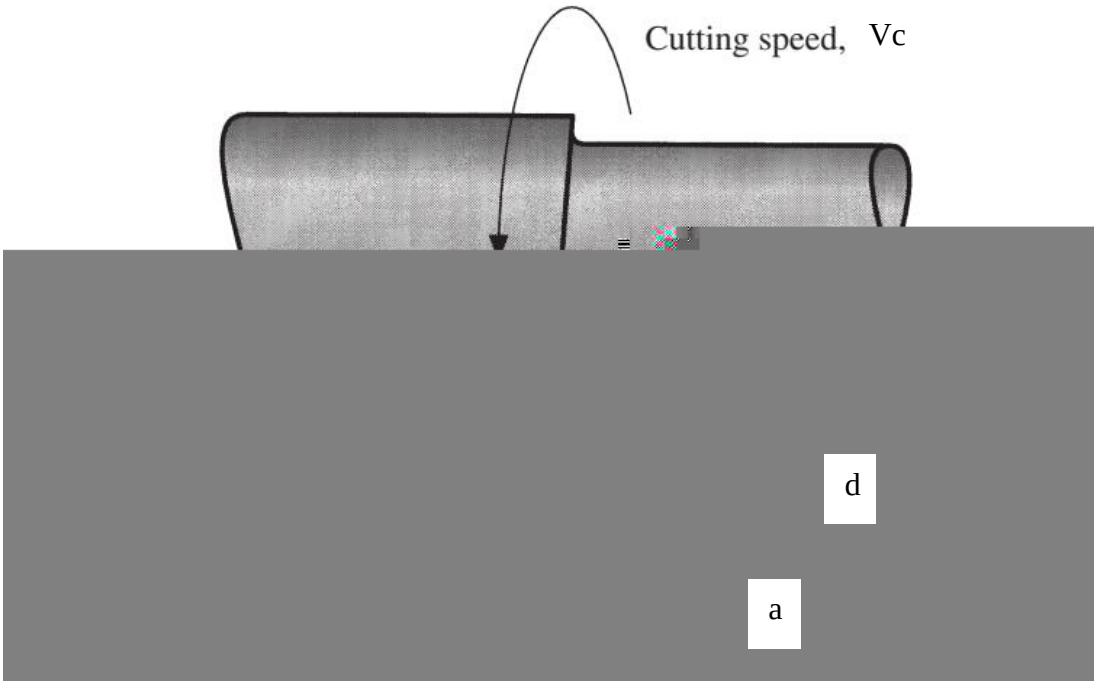

Fig. I.3: Cutting conditions [4]

I.3 Cutting Configuration

Since the geometry of a processes is complex. There is a simple modeling that will eliminate all the geometric complexity that is posed by the real model of the section called the orthogonal model. In fact, in reality, the models of the sections are three-dimensional but the orthogonal model presents the section in two-dimensional mode. This model is used to simplify the analysis of sections. Modeling is not used in industrial convontional machining. The second, more realistic model, called the oblique model, is used in conventional industrial machining. [4]

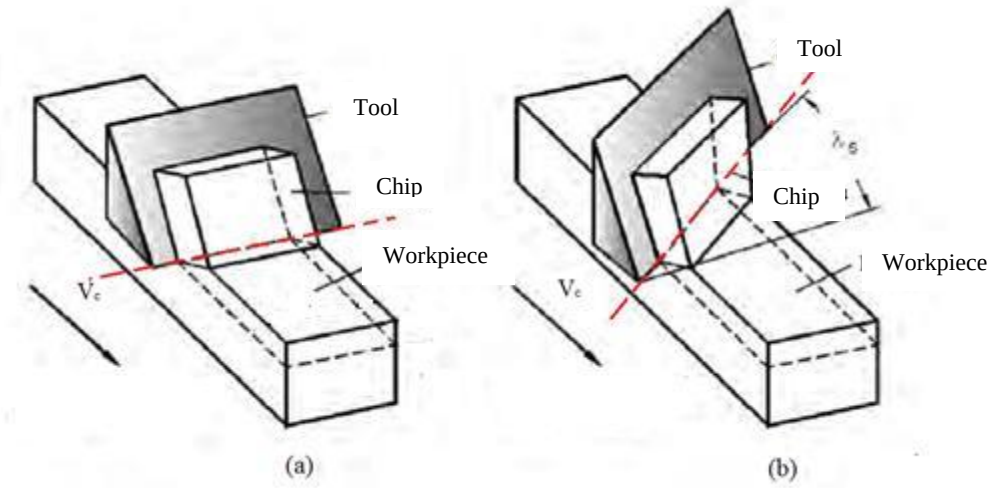

Fig. I.4: Illustrations of orthogonal cutting (a) and oblique cutting (b) [3]

I.3.1 Orthogonal Cutting

The cut is considered orthogonal when the cutting edge is perpendicular to the cutting speed. A large part of numerical and analytical models are based on the orthogonal model. [3] An orthogonal cut is an ideal cut that assumes that the material is completely homogeneous.

Most of the time, the orthogonal cut model allows to correctly approximate the performance of the sharp edge of the tool, which is why it is crucial to study it[5]. The majority of chip formation models have been developed for orthogonal cutting, although it is not widely used in industry. It will be used in the laboratory to understand the phenomena involved in cutting.

Its advantage lies in the simplification of theoretical research on the chip formation process, which makes the problem of plane deformations two-dimensional. [40]

I.4 Methods of measuring the temperature of during machining

It is clear that making mechanical parts by removing chips creates traction between the tool and the material. This pull increases the temperature of the tool. [7].

It is well known that when a part is turned into chips, significant amounts of heat are released due to energy transformations in the cut-off zone. The temperature that has been created is a crucial element that has the most influence on the process of transforming the machinery working layer into a chip. Also, it affects the phenomenon that occurs during the cutting tool wear (abrasive, adhesive, diffusive), The growth of temperature affects the magnitude of the cutting force components and causes residual stresses in different parts of the workpiece. That's why it's essential to know exactly what temperature is present in the cut-off area during the turning process.

The different zones of tool-workpiece contat during machining are as follows:

Main shear zone: it results from the change in the direction of the material's movement; This area is the site of intense shear and shear rates, which produce a high increase in temperatures due to dissipation [7].

Secondary shear zone: This area is exposed to high temperatures and high temperatures due to the friction of the chip on the tool.

Tertiary shear zone: In this zone, the tool exerts a compressive force on the retained material and divides it into two parts: the chip and the machined part. The formation of added edges is favoured by the presence of a chamfer between the face of the section and the face of the flank in this retention area.

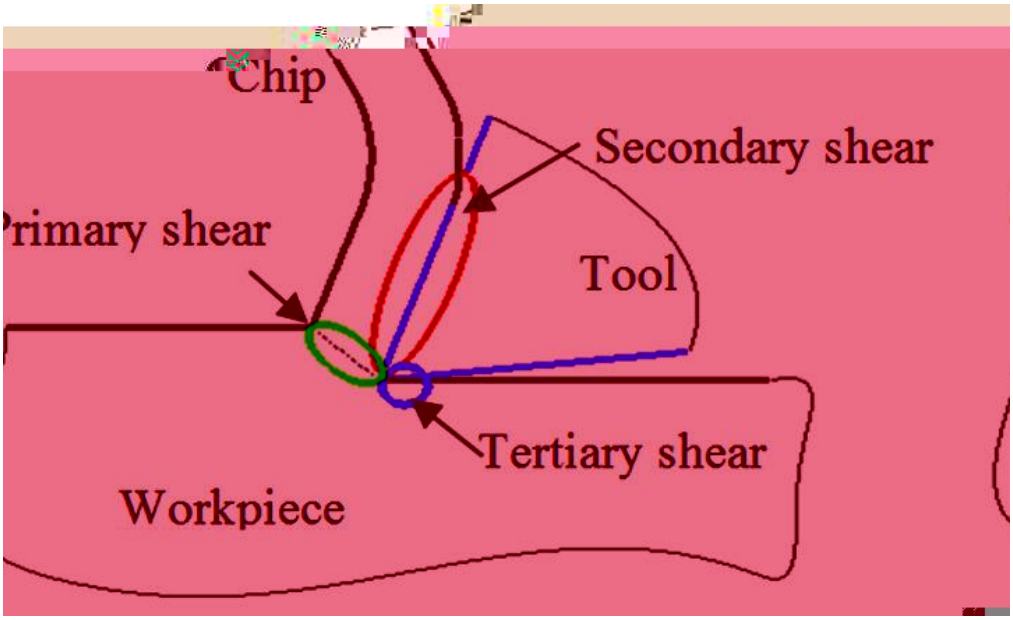

Fig. I.5: Different zones of chip formation [43]

Over time, a large number of heat and temperature measurement methods used in various manufacturing processes and tribological applications have been developed.

I.5 Cutting temperature measurement techniques

They include the following:

- dynamic and integrated thermocouples
- infrared photography
- infrared optical pyrometers
- thermal paints,
- materials with known decomposition temperatures, both powder and thin coatings
- temperature changes in the microstructures of high-speed steel tools. [8]

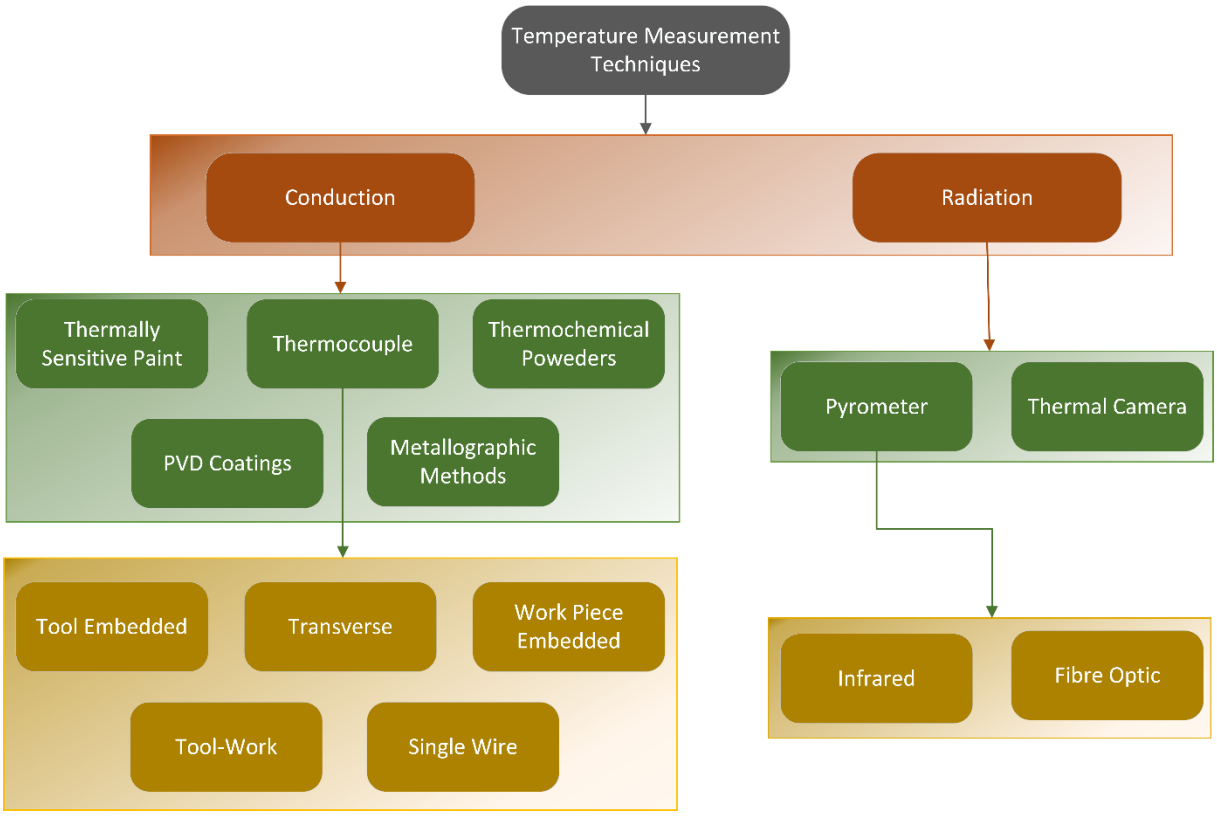

Fig. I.6: Temperature measurement techniques based on Byrne [31].

I.5.1 Thermocouple method

A thermocouple uses the principle that when two different metals are joined together to form two junctions, an electromotive force (emf) exists across the two junctions if they are maintained at two different temperatures (the hot junction and the cold junction). The materials used for the thermocouple and the temperatures at the junctions determine the EMF generated. The temperature ranges for some thermo-standard pairs are presented in Table 1 [41].

The following three thermoelectric laws that apply to thermocouples are as follows [9]:

In a thermoelectric circuit, the emf is independent of the system's component parts' grades and solely depends on the temperature differential between the hot and cold junctions; The size and resistance of the conductors have no bearing on the emf produced;

A third metal that is used to create the junction between the first two metals at the same temperature has no effect on the electromagnetic field generated if the junction of the first two metals is at a uniform temperature.

Table. I.1: Standard thermocouple types[9]

SLD[a]	Popular name	Materials (color code) (positive material appears first)	Typical temperature range	Seebeck coefficient at 100°C (212°F), μV/°C
S	–	Platinum–10% rhodium vs. platinum	−50 to 1767°C	7.3
R	–	Platinum–13% rhodium vs. platinum	−50 to 1767°C	7.5
B	–	Platinum–30% rhodium vs. platinum–6% rhodium	0 to 1820°C	0.9
T	Copper–constantan	Copper (blue) vs. a copper–nickel alloy (red)	−270 to 400°C	46.8
J	Iron–constantan	Iron (white) vs. a slightly different copper–nickel alloy (red)	−210 to 760°C	54.4
E	Chromel–constantan	Nickel–chromium alloy (purple) vs. a copper–nickel alloy (red)	−270 to 1000°C	67.5
K	Chromel–Alumel	Nickel–chromium alloy (yellow) vs. nickel–aluminium alloy (red)	−270 to 1372°C	41.4
N	Nicrosil–Nisil	Nickel–chromium–silicon alloy (orange) vs. Nickel–chromium–magnesium alloy (red)	−270 to 1300°C	29.6

[a] Standard letter designation.

The following three thermoelectric laws that apply to thermocouples are as follows [9]:
In a thermoelectric circuit, the emf is independent of the system's component parts' grades and solely depends on the temperature differential between the hot and cold junctions; The size and resistance of the conductors have no bearing on the emf produced; A third metal that is used to create the junction between the first two metals at the same temperature has no effect on the electromagnetic field generated if the junction of the first two metals is at a uniform temperature.

Thermocouples have the following benefits[9]:

1. low cost;
2. simple construction;
3. flexibility in construction;

4. simplicity in operation and signal processing;
5. ease of remote measurement.

Thermocouples come in two varieties: dynamic thermocouples, also known as tool-work thermocouples, and embedded thermocouples. [9]

- **Embedded thermocouples**

Embedded thermocouples were among the first thermocouples used to estimate temperatures in a variety of manufacturing and tribological applications. To use this technique in machining, deep holes must be made in the stationary part, such as the cutting tool. Thermocouples are then inserted in various locations within the tool, some as close to the surface as possible. Because multiple holes can alter heat conduction into tools and limit tool strength, only a small number of holes (usually only one) can be drilled in any given tool.

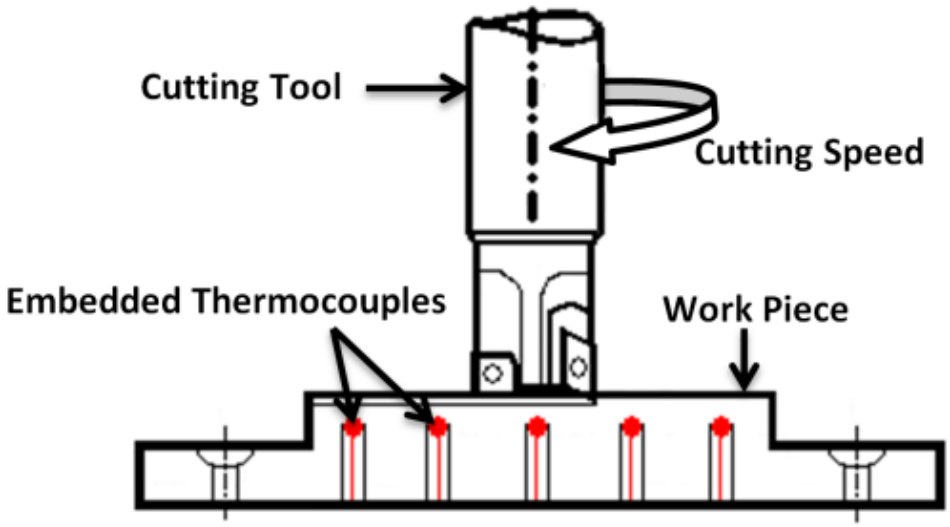

Fig. I.7: Embedded thermocouple [34]

The limitations of embedded thermocouples include the following: (a) Plotting temperature isotherms with embedded thermocouples in the tool can be time-consuming.

(b) Placing embedded thermocouples near the chip-tool contact region can be challenging and unsatisfactory due to heat flow interference. (c) The technique is challenging to implement due to the need for fine holes to locate thermocouples in difficult-to-machine materials like ceramics, cemented carbides, and hardened HSS tools.

(d) Temperature gradients at the surface are steep, making it difficult to locate two thermocouples close together. (e) Thermocouples have limited transient response due to mass and distance from intimate contact points. [9]

- **Dynamic thermocouples**

In the tribology literature, this method is frequently referred to as the Herbert–Gottwein technique [9]. In machining, two bodies in relative motion (in this case the cutting tool and workpiece) can be configured to form a thermocouple to measure temperature. This technique excels at analysing the impact of temperature on cutting parameters like feed rate and cutting speed. The method's limitation is that the accuracy of measured values is not absolute, making it only suitable for comparison purposes. Thermoelectric emf can be measured when dissimilar metals come into contact during cutting. The hot junction refers to the cutting zone, while the cold junction refers to an electrical connection between the tool and workpiece.

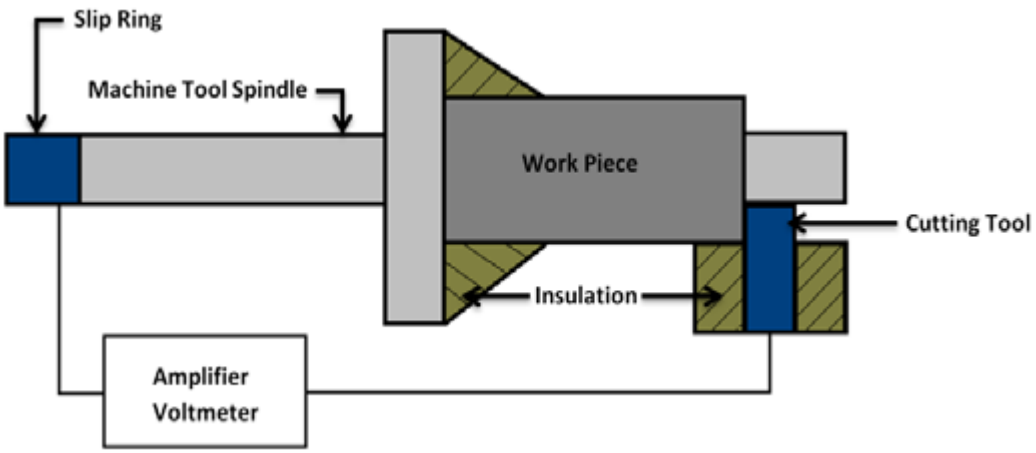

Fig. I.8: Schematic of a tool-workpiece thermocouple [35]

To employ this method on a standard machine tool, both the workpiece and the tool must be electrically insulated.[11]

Thermocouple applications are typically used to measure the average temperature in the cutting zone, rather than identifying thermal gradients caused by material non-homogeneities. The technique has proven effective in providing qualitative data and interface temperature trends together with their correlation with tool wear [12].

- **Single wire thermocouple**

The term 'single wire thermocouple' refers to a workpiece that has been cut into two sections across the cutting line. A thin insulated wire is also mounted through the workpiece. [10]

A signal is generated when the conductor's (thin wire) end comes into electrical contact with the work piece surface. During milling, the thin wire is cut, exposing it and forming a thermocouple with the cutting tool [11]. The signal lasts only during electrical contact with the wire, making it extremely short. A high sampling rate is used to record the signal during the brief measurement interval [13]. This method is similar to using an embedded thermocouple, sharing the majority of its advantages and disadvantages.

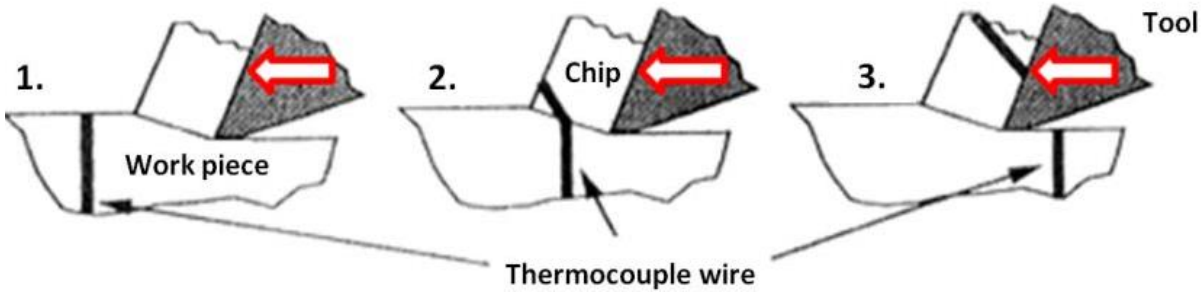

Fig. I.9: Illustration of a single wire thermocouple [35]

- **Transverse thermocouple**

Transverse thermocouples were used to investigate tool temperature distributions on the tool's end, clearance, and rake faces within the chip-tool interface area in three dimensions [9]. The method is similar to the tool/work piece thermocouple, with the exception that the contact point between the chip and tool changes constantly as the cutting progresses [9]. The thermo-electric junction is made up of the tool material and another material's sharp probe. With the displacement of the probe, a continuous temperature distribution relative to a specific edge is captured [9].

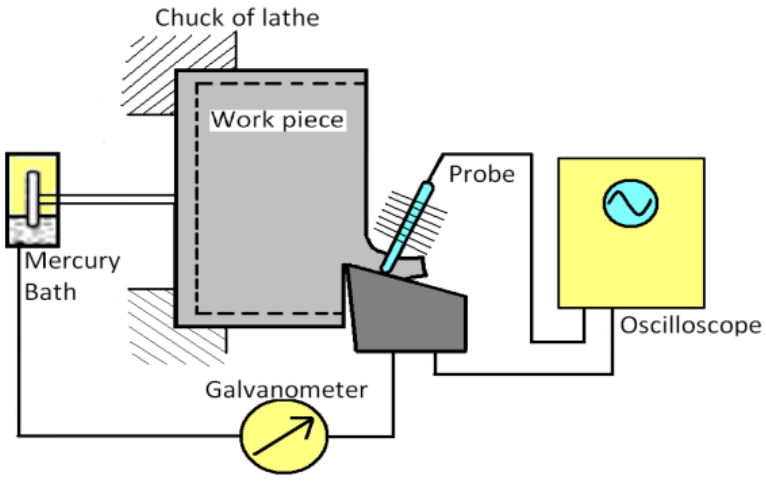

Fig. I.10: Transverse thermocouple illustration [9]

I.5.2 PVD coatings

The measurement method involves applying a PVD coating to a split-tool in an aqueous solution. Melted coatings indicate that temperature thresholds have been exceeded [16]. This method allows for the determination of a solid body's internal temperature during milling. Temperature detection coatings are physically vapor-deposited on the split surface of cutting tools using materials with varying melting points.

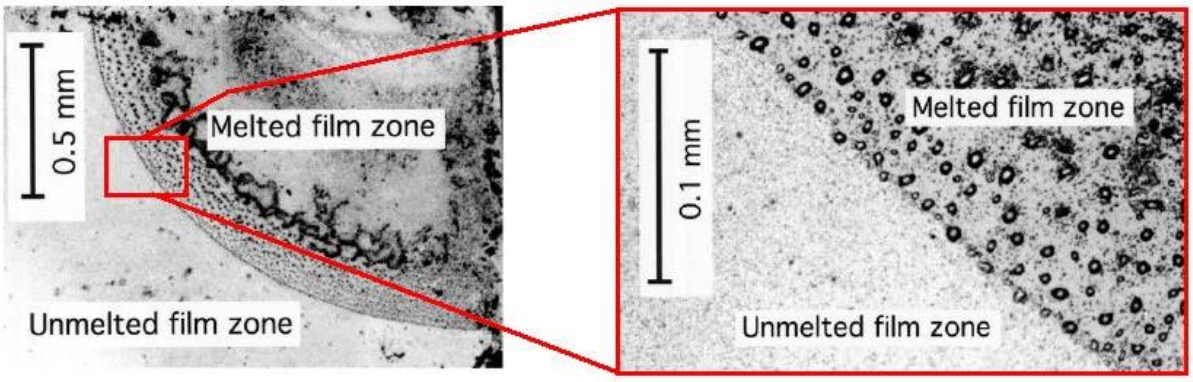

Fig. I.11: Melted and un-melted regions of tellurium coating with an isotherm of 723K. [9]

Table. I.2: Melting points of different PVD coatings[10]

PVD film material	Symbol	Melting Point [°C]	Purity
Tellurium	Te	450	99.999
Lead	Pb	328	99.999
Bismuth	Bi	271	99.999
Indium	In	157	99.99
Alloy*	Alloy	96.6	99.99

* Composition (wt %) Bi : Pb : Sn = 50 : 28 : 22

Each film material melts at a different temperature, and an image of the spatial distribution of temperature near the cutting edge is captured. Calibration tests can determine the precise temperature at the boundaries between the melted and un-melted films[16]. Boundary images are shown in fig.1.9. PVD coatings are known for their minimal impact on heat transfer and internal temperatures. Micrographic results provide clear binary interpretation, enabling accurate detection of temperature distributions. The PVD materials accurately map contours on the spatial domain, but limit the method to discrete sensing points on the temperature scale. This results in a stepwise detection method with limited resolution. The PVD film technique is not suitable for cooling as it damages the coating [10].

I.5.3 Thermo-chemical Powders

Similar to PVD coatings, temperature sensing involves observing the melting of the powder. This method separates the cutting tool into two parts with a symmetrical interface.

The interface is coated with powder during the assembly process. The temperature distribution is determined by repeating the experiments with different melting point powders one at a time[10]. Le tableau 10 énumère les poudres courantes ainsi que leurs points de fusion et d'ébullition [17].

Table. I.3: Melting amd boiling points of different thermo-chemical powders[10]

Chemical substance	Melting point [°C]	Boiling point [°C]
NaCl	800	1413
KCl	776	1500
CdCl	568	960
$PbCl_2$	501	964
AgCl	455	1550
Zn	419	907
KNO_3	339	-
Pb	327.4	1750
$SnCl_2$	246.8	623
Sn	231.9	2270

As results are obtained for one type of powder at a time, they are combined by superimposing the boundary lines of the various tests to determine the temperature isotherms [10]. Microscopic analysis allows for clear visual distinction between melted and un-melted zones, improving repeatability [10]. Chemical powders are a reliable method for detecting temperature due to their consistent melting points and visible change. A constraint is the number of times each temperature is sensed. High pressure cooling is not effective as it removes powder from the interface. [10]

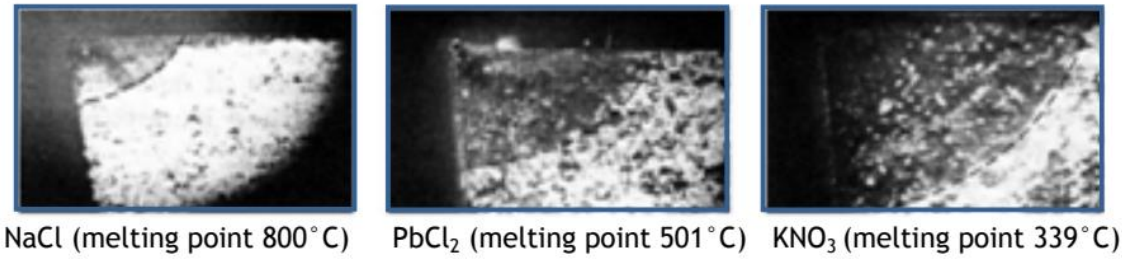

Fig. I.12: Images of sandwich surface tools where the use of NaCl, $PbCl_2$ and KNO_3 [9]

I.5.4 Radiative temperature measurement methods

Non-contact, or radiative, measurement techniques interpret and measure the thermal energy, in the form of infrared (IR) radiation, emitted by an object of interest to determine its thermodynamic temperature based on the wavelength of the emitted radiation [23,24]. This often allows for non-intrusive temperature measurements to be taken from a distance [25].

The energy that matter emits electromagnetically above absolute zero is known as thermal radiation [5]. An object's temperature and emissivity determine how much heat radiation it emits. A material property called emissivity (ε) is the ratio of a body's radiation to that of a black body at the same temperature.

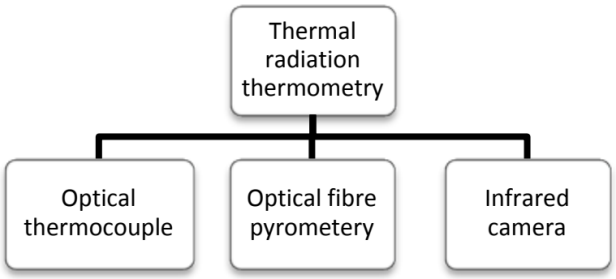

Fig. I.13: Radiative methods of temperature measurement

It is common practice to use the object's temperature ascertained by the thermal radiation method in conjunction with an accurate thermocouple measurement of the object's temperature to calculate emissivity. The precision of thermal radiation temperature readings is directly related to the emissivity's accuracy. It is extremely important to interpret instrument-based readings with extreme caution because emissivity varies with temperature and the presence of an oxide layer. As a result, radiation thermometry for machining is now more related to science than to industry.[10]

Emission in the infrared band, which is used in radiation thermometry, is defined as from the visible red light's edge at 0.74 μm to 300 μm (frequency 1 to 400 TeraHz).[10]

- **Infrared Camera**

These days, thermal cameras can capture process thermal images in real time at very high frame rates. An IR camera must have a direct line of sight to the area of interest in order to measure the area, as shown in the diagram below[22]

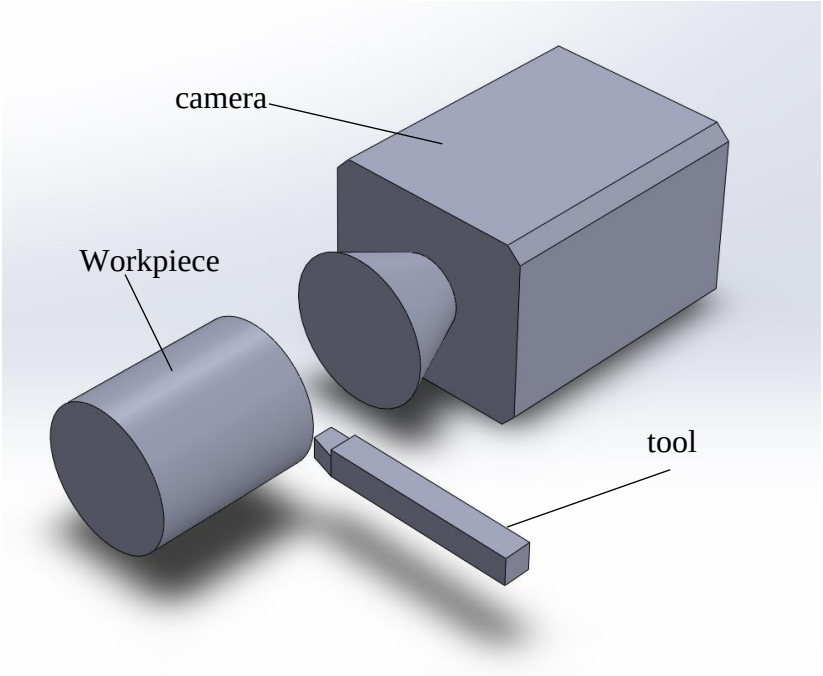

Fig. I.14: Infrared camera temperature recording configuration.

Without changing how heat is distributed within the materials, the IR-camera approach allows for non-destructive means of obtaining and analyzing the temperature-distribution map of the area of interest. It can also be used repeatedly without wearing out mechanically[22].

Fibre Optic Infrared Thermometers

A fibre is used in a FOIRT to receive and transfer radiation emissions to a photosensitive detector [9]. A fibre is used in a FOIRT to gather and transfer radiation emissions to a photosensitive detector. By positioning the fibre closer to the area of interest, a fibre-optic infrared thermometer can reduce problems with line-of-sight disruptions and emissivity uncertainties brought on by reflected radiation. Furthermore, by positioning FOIRTs away from the target with the radiation emitted and transmitted by the fibre, they can better shield the electronics from the harsh machining environment.

- **Infrared thermometers**

The principles and methods of operation of infrared thermometers (IRTs) and infrared cameras are similar. IRTs and IR cameras differ primarily in that the former measure temperature at a single point and average the observed area's temperature, while the latter create a temperature map. [22] The incoming radiation from within the IRTs' field of view is focused by lenses onto a detector, which measures the average temperature of the region observed. To accurately locate the area of interest, IRTs are frequently fitted with a laser as a guide. Without requiring physical contact, IRTs have extremely quick response times and can measure temperature accurately. Because of these features, IRTs can be used for high-speed machining applications, particularly interrupted machining processes where the tool's temperature can change at very high intervals in a way that is proportionate to the cutting speed.

Fig. I.15: Image of a typical infrared thermometer [36]

Conclusion

Machining processes can generate an enormous amount of hear from the interaction between the cutting tool and the workpiece. In order to create new cutting materials, we need to understand how cutting conditions affect the cutting the temperature. Numerous methods can be employed to record the cutting temperature, no method is perfect. Each has it's own strength and weaknesses and is well suited for a particular use case.

CHAPTER II: Infrared camera

II.1 Introduction

Due to the significant advancements in IR detector design, electronics, and computer science over the past three decades, infrared (IR) thermal imaging, or thermography for short, is a rapidly developing field in both science and industry [26]. These days, thermography is used in many different areas of industry and research, including non-destructive testing, condition monitoring, predictive maintenance, lowering the energy costs of buildings and processes, gaseous species detection, and many more.

An IR camera's primary function is to transform infrared radiation into a visual image with false colours, including grayscale [26]. The two-dimensional distribution of infrared radiation emitted by a scene or an object should be represented by this visual representation. The visual image for a temperature-measuring system shows the object temperatures. Thus, the optics, detector, cooling or temperature stabilization of the detector, electronics for signal and image processing, and user interface with output ports, control ports, and image display are the main parts of an infrared camera.

II.2 Infrared Thermography

Infrared thermography is a remote measurement technique that uses the characteristics of infrared light [27]. A thermogram, which is a measurable snapshot of a static or dynamic thermal phenomenon, is created using this method to obtain a heat map.

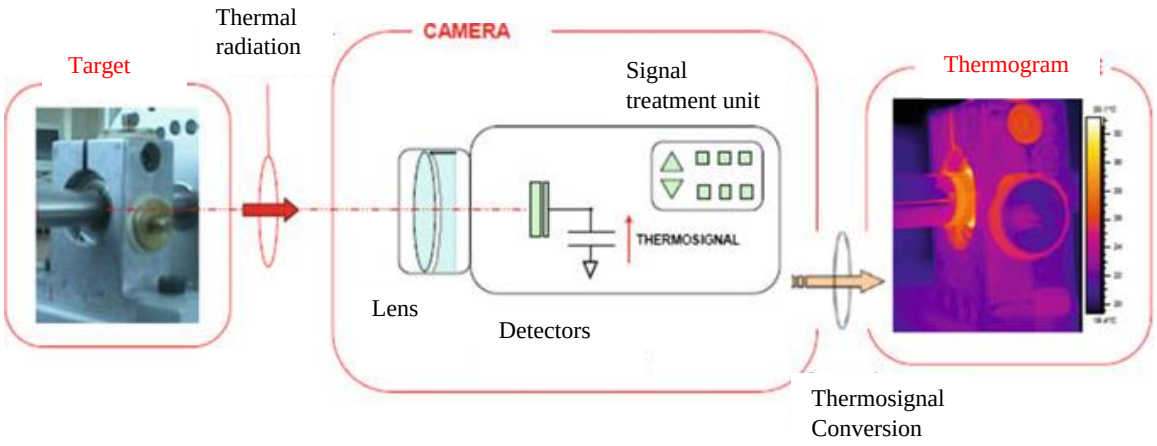

Fig. 2.1: A sequence of processes of capturing athermogram [7]

An infrared camera, also known as a thermographic camera, infrared measuring camera, or thermal analyzer, is the measuring tool.

II.3 Thermal radiation

In infrared thermography, we generally work in a spectral band of 2 to 15 µm. Visible light, ultraviolet radiation and infrared radiation are described as electromagnetic waves. Infrared radiation is produced when an object's temperature rises above its thermodynamic absolute zero (0 Kelvin) temperature[30]. Thermal radiation is a type of electromagnetic waves found in the Infrared Radiation spectral region.

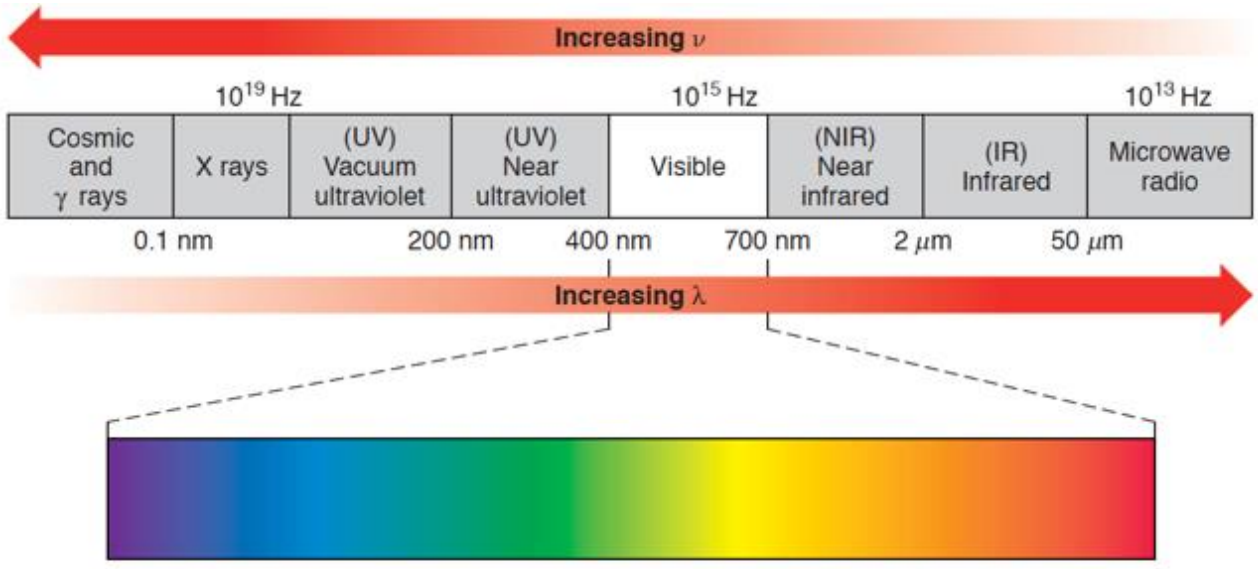

Fig. 2.2: Infrared spectrum [39]

The oscillation of an electric field and a magnetic field produces an electromagnetic wave. The two fields, which are perpendicular to each other, propagate at a speed that depends on the medium in question [28]. An electromagnetic wave is characterized by its wavelength **λ**(m), its period T(s) and its frequency **ν**(Hz) which is a reciprocal of the period **(ν = 1/T).**

The propagation speed c is related to the wavelength and the frequency by the following formula:

$$\mathbf{c = \lambda \cdot \nu}$$

II.4 Emissivity

An object's emissivity can be defined as the ratio of the actual radiation emitted from its surface to the radiation produced by a blackbody at the same temperature [26]. The straightforward relation that provides the relationship between reflectivity and emissivity for opaque bodies is given by [29]:

E + R = 1

In which case E is for emissivity and R is for reflectivity.

II.4.1 Factors affecting emissivity

Compared to no metallic objects like wood and paints, metallic objects are particularly difficult to work with. Owing to their low emissivity values which are as low as 0.2 [26].

Irregular Surface Structure:

Because of the surface structure, the emissivity of any given material can vary greatly [26]. This results in the undesirable circumstance where a wide range of emissivity values are reported for the same material. Metals are most prominently affected by this effect.

While some polished metals can have ε values as low as 0.02; however, if the surfaces are roughened, the emissivity can be much higher and even exceed 0.8. The values of emissivity can be greatly improved by surface imperfections such as corrosion over time.

Viewing angle:

When it comes to radiation emissions, blackbodies exhibit perfect isotropic behaviour, meaning that the radiation's radiance remains constant regardless of its direction of emission [26]. However, the behaviour of a real surface varies, meaning that its radiance changes based on the direction of emission.

The diagram below shows how viewing angle can affect the resulting thermograph from an infrared camera

Regular Surface geometry:

Surface structure and geometry are related; however, regular surface geometry refers to well-defined geometric structures like grooves, which are used to systematically change emissivity, as opposed to irregular surface roughness[26].

Wavelength:

In optics, it is well known that wavelength typically affects a material's properties. Take the reflectiveness of the noble metals copper (Cu), silver (Ag), and gold (Au), for instance[26]. The distinctive reddish-brown and golden-yellow colours of Au and Cu are ultimately caused by wavelength-dependent reflectivity resulting from their electronic inter-band transitions in the visible spectrum. Since emissivity and reflectivity are closely linked, any wavelength dependence on reflectivity will also manifest itself in emissivity.

Temperature:

It should come as no surprise that emissivity changes with temperature as other material properties do[26]. Since some materials exhibit fairly large variations, it might be important to determine whether a process's temperature under infrared observation will stay within a given temperature range so that the emissivity for this study can be regarded as constant for practical reasons. Furthermore, one needs to be aware of the matching temperatures if the emissivity values from the literature are to be used.

II.5 IR imaging system

Thermal imaging systems consist of: optical system, the infrared detector, the electronic information processing system, and the display system, which make up the system's main parts[30]. The optical system's job is to concentrate the infrared rays that are received onto the photosensitive components of the infrared detector, as seen in the figure below. Infrared radiation is transformed into an electrical signal by the infrared detector. It serves as the thermal imaging camera's central component. Electronic information processing systems are responsible for the amplification and processing of electrical signals. On a monitor or LED screen, the display presents the electrical signal as a visible image.

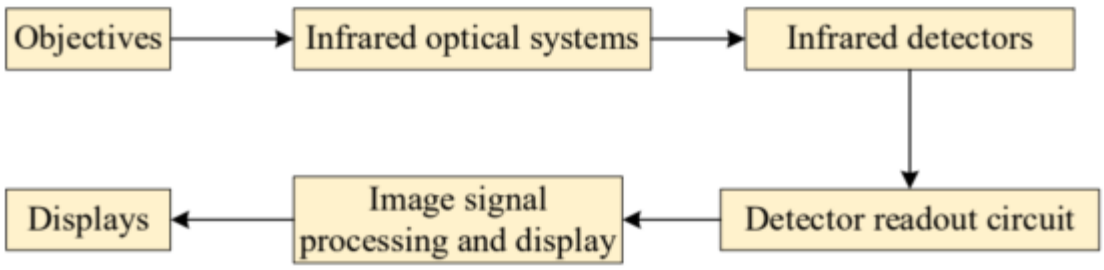

Fig. 2.3: Components of an infrared camera[30]

II.6 Working of an infrared camera

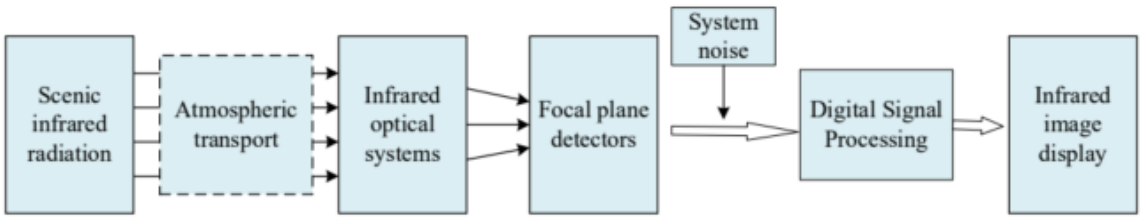

Fig. 2.4: The process of capturing and displaying a thermogram [30]

The focal plane thermal imaging camera's detector shape is two-dimensional. Infrared light is focused on the plane of the infrared detector array by passing the target to be measured through a straightforward objective lens; this process is essentially analogous to the principle of photography. Figure below illustrates the imaging concept.

The infrared thermal camera captures a dark image with low contrast between the target and background, fuzzy edges, and low resolution. The accuracy of temperature measurement is low because of the limitations of both the equipment used and the external environment. The image captured by the infrared thermal imager needs to be processed in order to increase accuracy because of the influence of different noises. The use of algorithms helps correct, denoise, and enhance the non-uniformity of the image to improve temperature measurement accuracy, contrast, resolution, and signal-to-noise ratio.

II.7 Calibration of the infrared camera

The process of imaging a calibration target with geometrically known features in order to ascertain the intrinsic and extrinsic parameters of a camera is known as geometric calibration. The values of a camera's interior orientation components, such as the focal length, skewness, principal points in image coordinate systems, and most importantly he radial and tangential distortions brought on by the lens, are known as intrinsic parameters [16–18].

On the other hand, a 3D geometric scene can be transformed to the camera's 3D coordinate frame using extrinsic parameters. This makes it possible to represent the camera's spatial location in a 3D scene and makes measurements in world coordinates possible. [6]

Typically, visible camera calibration is carried out with the widely used checkerboard pattern, which is produced with low-cost, off-the-shelf printers [20–23]. Since visible and infrared cameras operate in different spectrum bands, infrared cameras are unable to display the visible colour of an object they are imaging.

Because the checkerboard pattern's features are invisible at room temperature to IR cameras, using the standard paper-printed checkerboard pattern to calibrate visible cameras for the calibration of infrared cameras is not appropriate [24].

Consequently, calibration targets for IR cameras will have unique characteristics in the IR spectrum due to variations in materials they are made from, surface emissivity, and thermal conductivities, enabling the geometric calibration of IR cameras [26].

II.7.1 Geometric calibration targets

Passive and active calibration targets are the two types of thermal camera geometric calibration targets [26]. The difference in emissivity values of the pattern is the primary criterion for passive targets, which can also make use of an external heater to make the pattern visible in the infrared spectrum. Sources of external heat can include sunlight, fluorescent lamps, and electric fans that operate independently of the calibration target.

On the other hand, active targets amplify the contrast in a thermal image by utilizing both the emissivity difference and an integrated heater[26]. Because active targets need electrical work in addition to the chosen pattern, this makes the fabrication of the calibration target more difficult.

Since this is a field of active research, many advancements using various methods and calibration targets to geometrically calibrate infrared cameras are constantly being made and published.

II.7.2 Calibration techniques

Square checkerboard technique:

The common square checkerboard pattern printed on paper using ink and/or laser technology is one of the most widely used methods for calibrating visible cameras[32]. Nevertheless, an external source of radiation such as a flood lamp is used to heat the pattern, making it visible in the infrared range [27, 28].

Numerous studies using different materials with varying emissivity coefficients for the checkerboard elements have been done but the fundamental idea remains the same. Heating the checkerboard to with an IR emitter or floodlamp to allow for detection of the calibration target using the infrared camera.

Circular board technique:

To calibrate thermal cameras, circular patterns with symmetrical and asymmetrical configurations have been developed in the literature in addition to the straightforward square checker patterns [32]. The manufacturing and recognition algorithms for circular calibration targets are typically complex, requiring specially designed codes in order to identify the circular pattern and determine its centre points. Nevertheless, compared to square or checker patterns, such circular calibration targets typically produce better calibration results [6]. Since the algorithm follows the circular patterns to estimate their centre points and uses them as control points.

Conclusion

All the bodies emit radiation with a range of wavelengths, part of the spectrum of wavelengths emitted by bodies above the absolute zero temperature can be harnessed with infrared camera technology to give information such as the body's temperature and shape. Infrared technologies can be used in domains such as military and infrared security to mansion just a few.

Before infrared cameras of sensors can be used, the need to be calibrated to be well adapted to their destined environment.

Chapitre III**: Experimental part**

III.1 Introduction

The purpose of this chapter is to present the various experimental methods and techniques that were employed during this study.

All materials used in this study were obtained from the university's workshop. The material used was obtained from an aluminium alloy cylindrical bar of 50mm in diameter. A tool made of steel P20 was used during the experiment, on a lathe machine with variable speed.

To record the temperature, we used the FLIR SC305 infrared camera. The camera signal was treated by FLIR Thermal Studio Suite to give numerical results. The numerical results were treated by Minitab to trace curves and make tables.

The main process involved in the experimental phase is the treatment of the Aluminium alloy parts using matte black paint to increase emissivity, the setting up of the tool and aluminium parts on the lathe machine. We also set up of the camera on the lathe machine to have a clear field of view so as to record the contact point between the tool and workpiece.

Once this is done, the machining process could be recorded by the camera and data is sent to a computer, via an Ethernet cable, where it is saved.

III.2 Experimental study

III.2.1 Presentation of materials

Machine-tool

A parallel lathe is a machine tool that rotates a workpiece around an axis of revolution, enabling the formation of new geometries through material removal. The lathe we used for this study is from the brand TOS TRENCIN. The range of the turning speed of this lathe is 22.4tr/min to 2000 tr/min. The cross-sectional feed rate of this particular model ranges from 0.05 to 6.4 mm/tr.

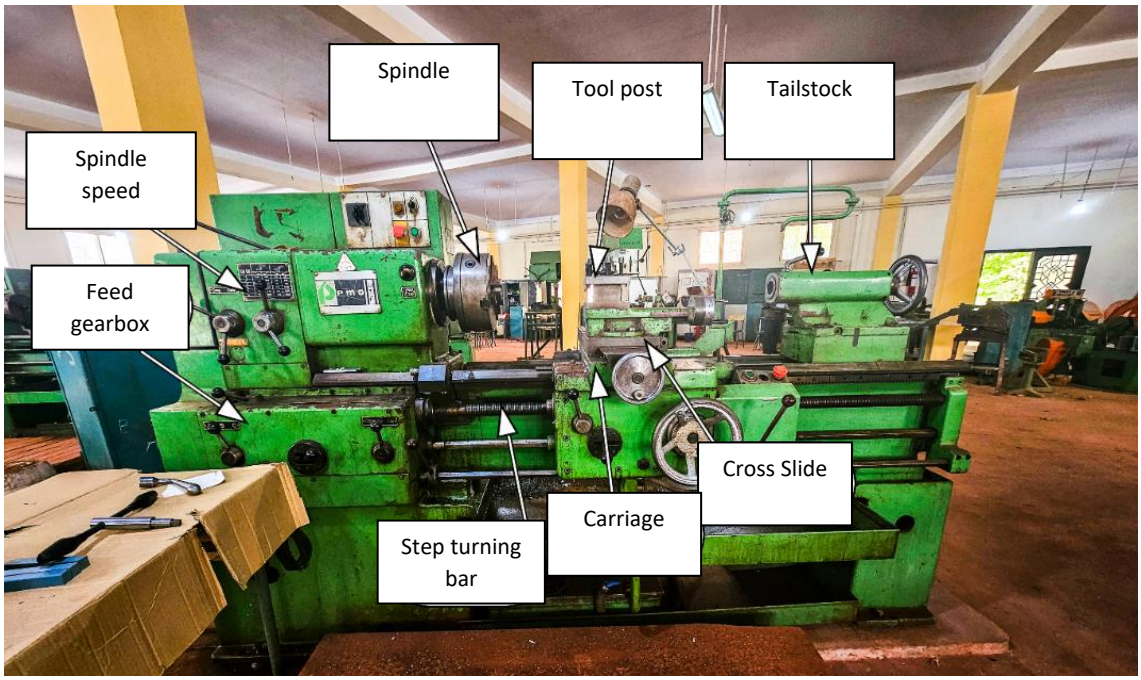

Fig III.1: Parallel lathe characteristics

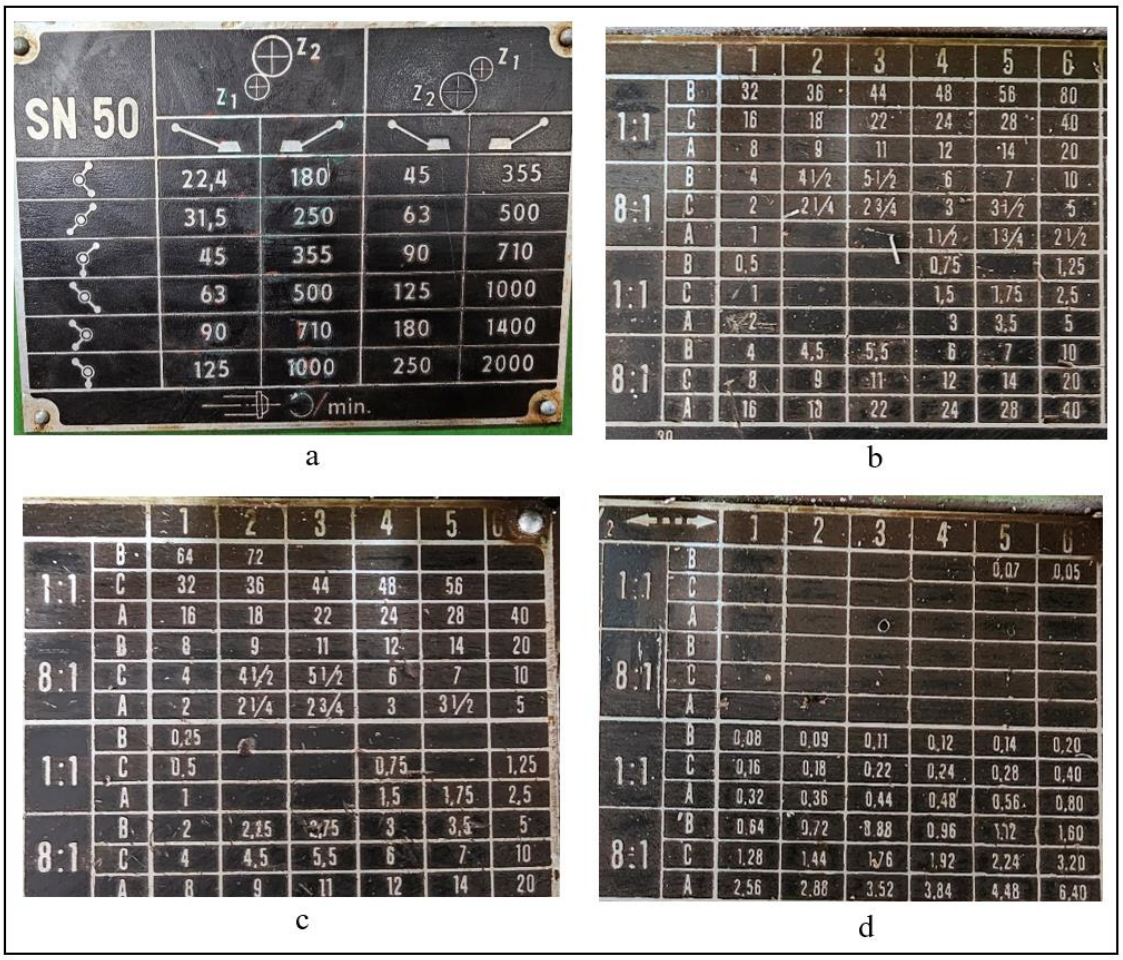

Fig III.2: Cutting speed and feed rate characteristics of the parallel lathe

Cutting Tool

The figure below shows the image of the facing tool used in the experiment.

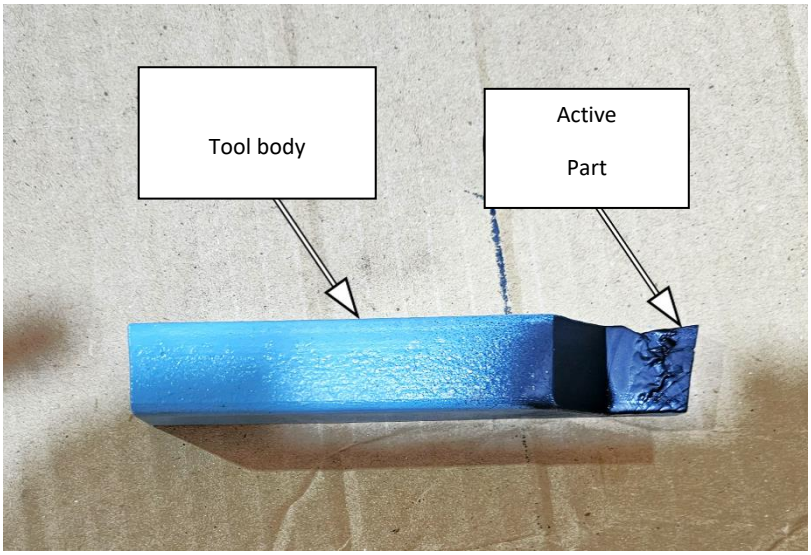

Fig III.3: Cutting tool

Raw parts

In this experiment, we used cylinders of 50mm in diameter and 60mm in length, made of aluminium alloy cut from a cylindrical bar using a band saw sawing machine.

Fig III.4: Unmachined parts

To cut the workpieces, we used a bandsaw sawing machine, **Pehaka Roboter 250**, with the following characteristics:

- A **2.2-Kilowatt** electric motor
- **4100mmx34mmx1.1mm ribbon**
- And a ribbon speed of **20-80m/minute**
- Weight: **750kg**
- Cutting capacity at 90º: **round:330mm**, **square:330x330mm, rectangle 300x480 or 225x530**
- Cutting capacity at 45º: **round:275mm**, **square:270x275mm, rectangle 300x275**

Fig III.5: Pehaka Raboter 250

A band saw machine with a toothed metal blade that can be rectilinear or circular in shape is used hard materials with an alternating or rotating movement. The machine can be distinguished based on the type of tool used:

Band saw sawing machines, which use a very long blade with one edge fitted with teeth and whose ends are welded; Reciprocating sawing machines, also known as oscillating sawing machines, whose tool consists of a straight toothed blade driven by a reciprocating rectilinear movement. The image below shows the machine used in the cutting process.

Fig III.6: Cutting the aluminium alloy workpiece on a band saw

The infrared camera used

The infrared camera used in this study is the FLIR SC305. With a resolution of 16 bits, the camera can stream thermal images made up of 76800 distinct pixels. The camera's optics and uncooled microbolometer detector enable 25° x 18.8° observations. The detector has a spectral range of 7.5 to 13 µm and a pitch of 25 µm.

Table III.1: Characteristics of the Flir Sc305 infrared camera. [42]

Image and optics	
Field of view	25º x 18.8
Minimum focus	0.4 m
Focal length	18mm
Thermal sensitivity	50mK
Image frequency	9Hz
Detector	
Type of detector	Focal Plane Array (FPA), uncooled microbolometer
Spectral range	7.5 - 13 µm
Image resolution	320 x 240 pixels
Detector pitch	25 µm
Measurement	
Accuracy	±2°C or ±2% of reading
Object temperature range	-20°C to +120°C 0 to +350°C

Fig III.7 : Flir 305Sc infrared camera

III.2.3 Mounting the camera

The camera is mounted at a distance of 30cm away from the point of contact between the tool and workpiece in such a way that the cutting edge of the tool is within the field of view of the camera.

This ensures that the cutting edge of the tool remains in focus even as the feed changes.

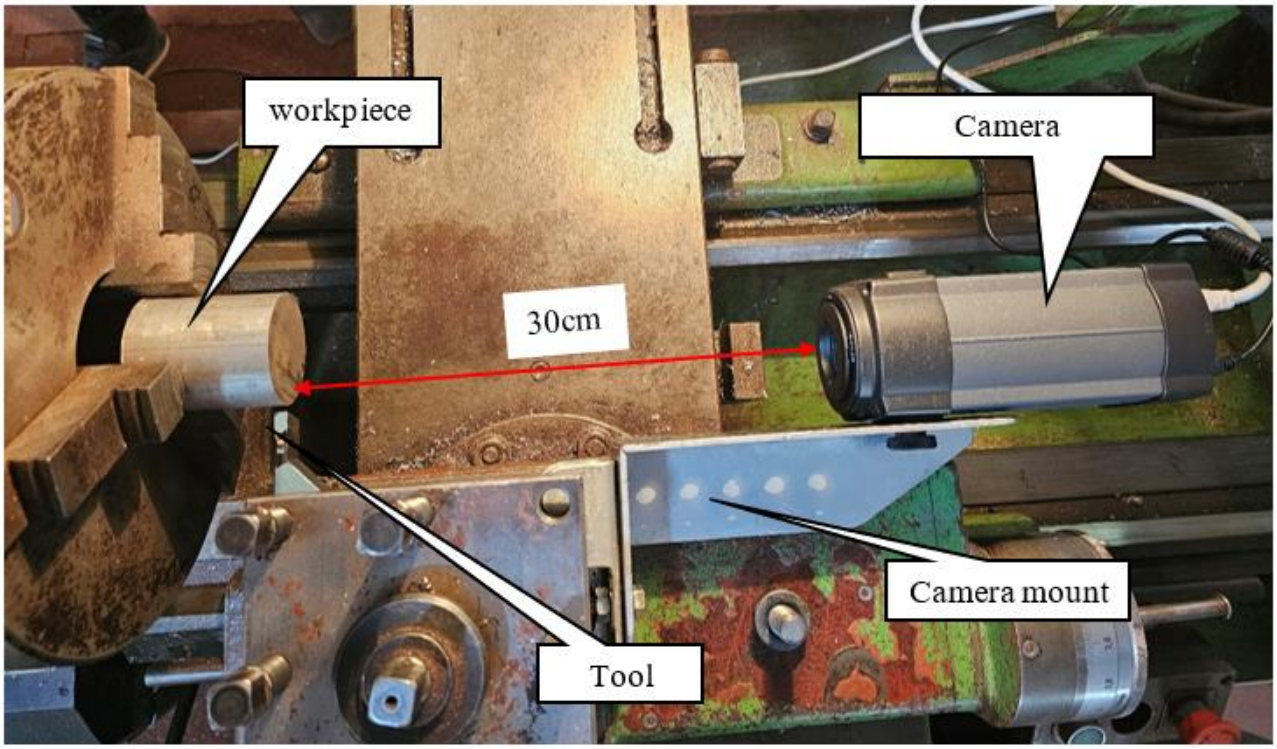

Fig. III.8: Camera mounted on the turret 30cm away from the cutting edge of the tool.

The camera was attached to a turret that accommodates the cutting tool using an adjustable camera mount to ensure that the focus point of the camera moves together with the tool as shown in

Fig. III.8.

III.2.4 Camera Software

We used a computer to treat the camera signal, with the help of the Flir QuickPlot software. The first step when using the software is saving the video sequence, followed by the analysis of recorded images to determne the temperature.

Software interface

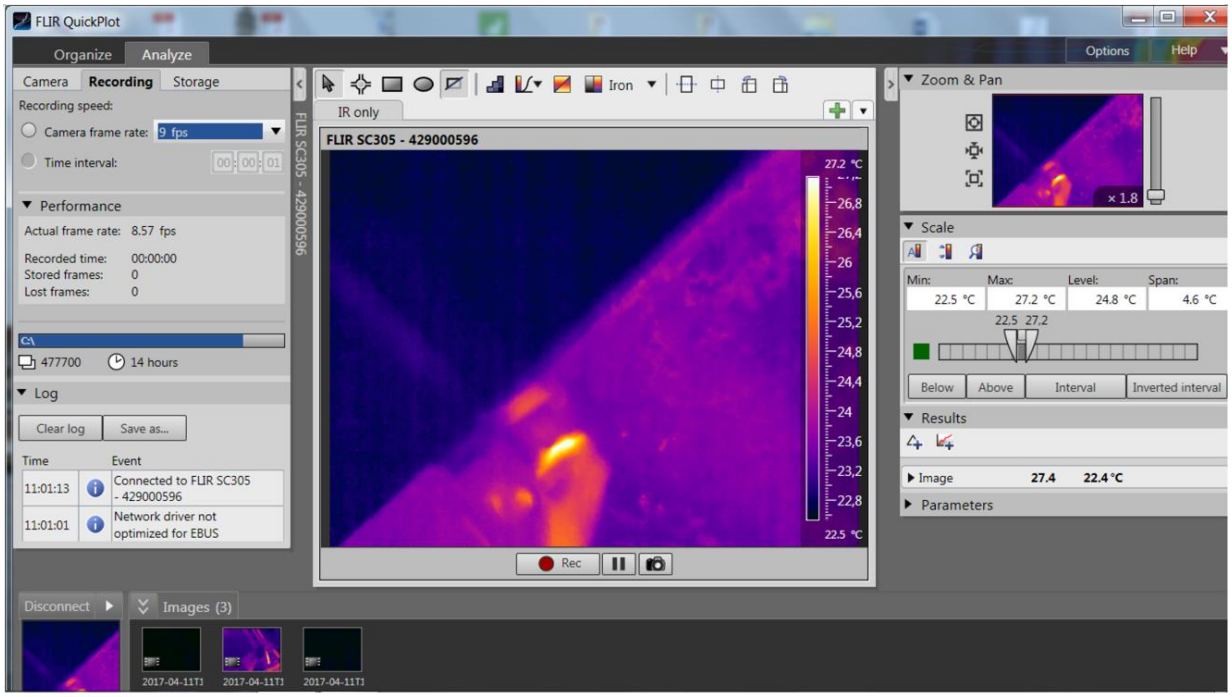

Fig III. 9: Image of Flir QuickPlot interface

The different parts of the software's user interface are as follows:

Main Tabs

This bar contains analytical and organisational functions of the Flir Quickstep software.

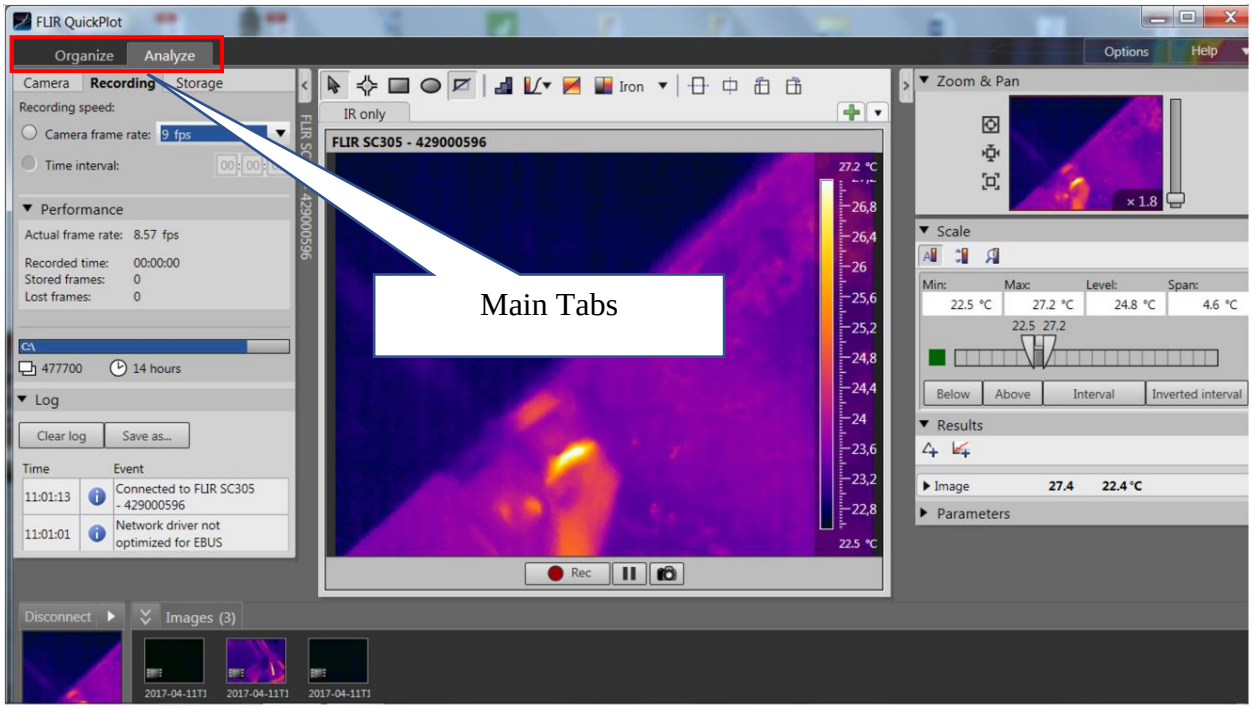

Fig III.10 a: Main tabs of the Flir QuickPlot Software

Sub tabs

A group of recording, storage and camera settings tabs.

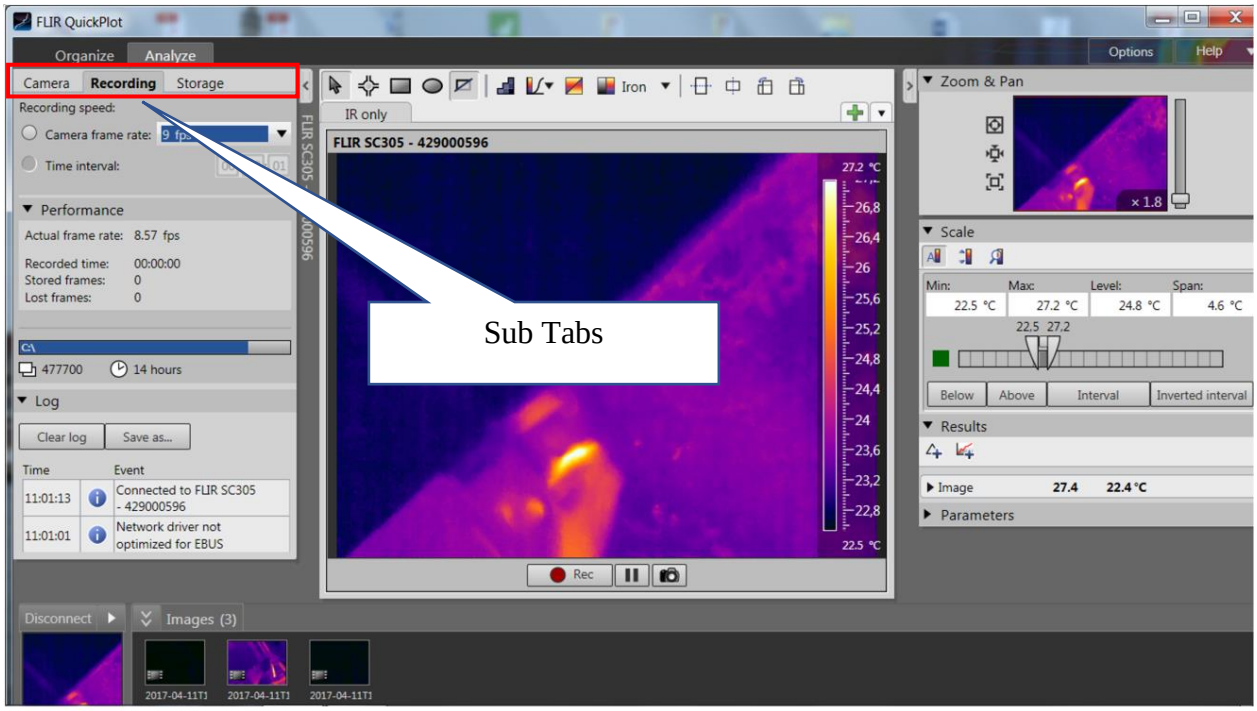

Fig III.10 b: Sub-tabs of the Flir QuickPlot software

Toolbar

Contains different tools for image analysis such as isotherms and selection of specific zones.

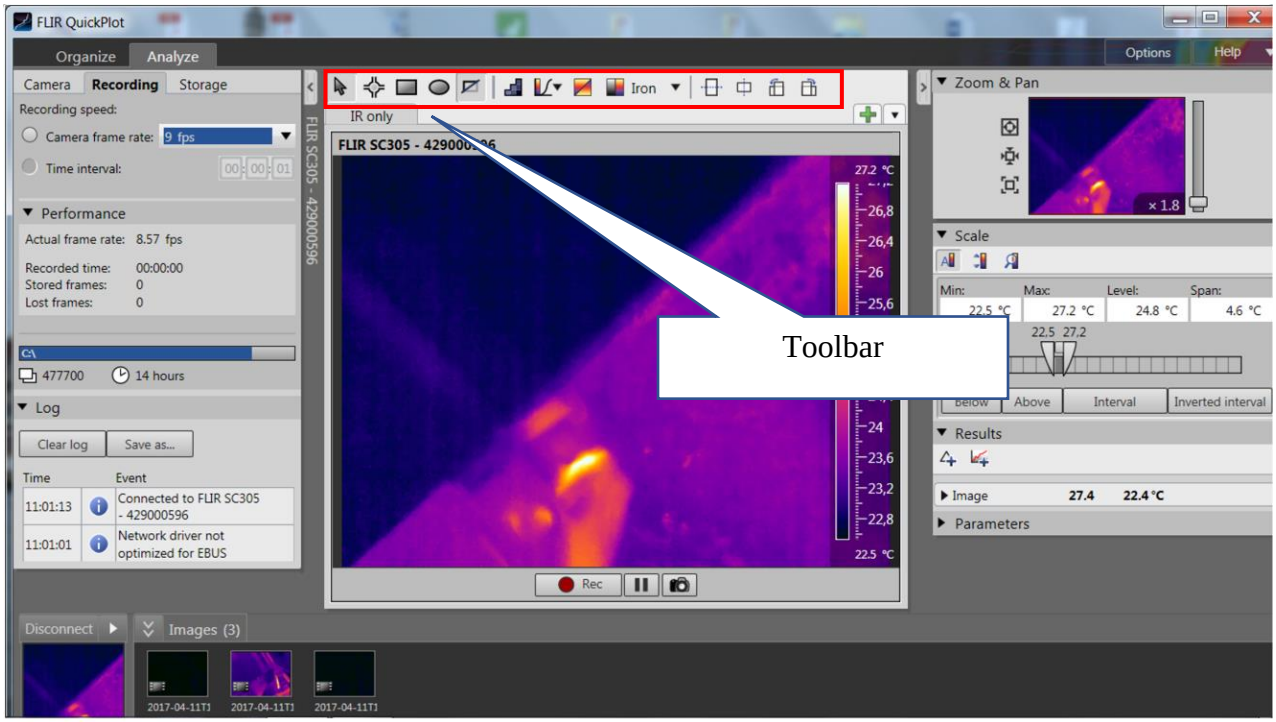

Fig III.10 c: Sub-tabs of Flir QuickPlot

Image window: Displays live signal from the camera.

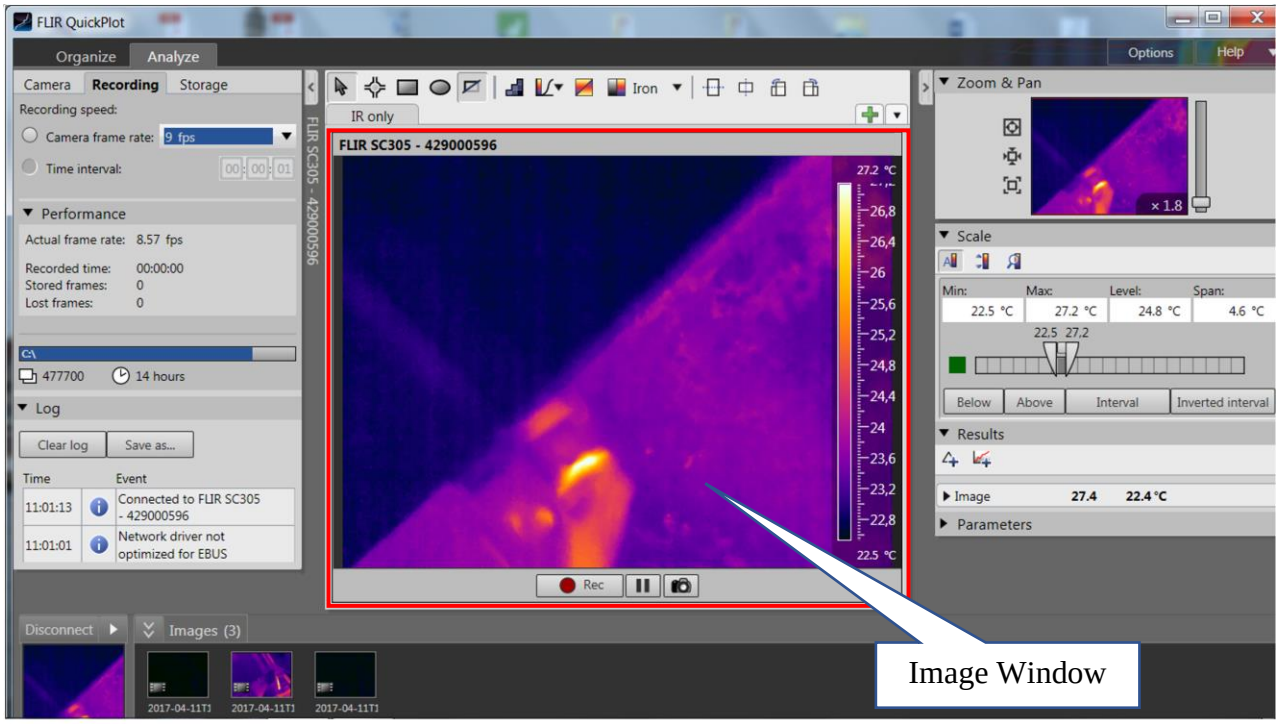

Fig III.10 d: Image window of the Flir QuickPlot

Add button

Used to select and add more tabs to the image display window from the dropdown menu.

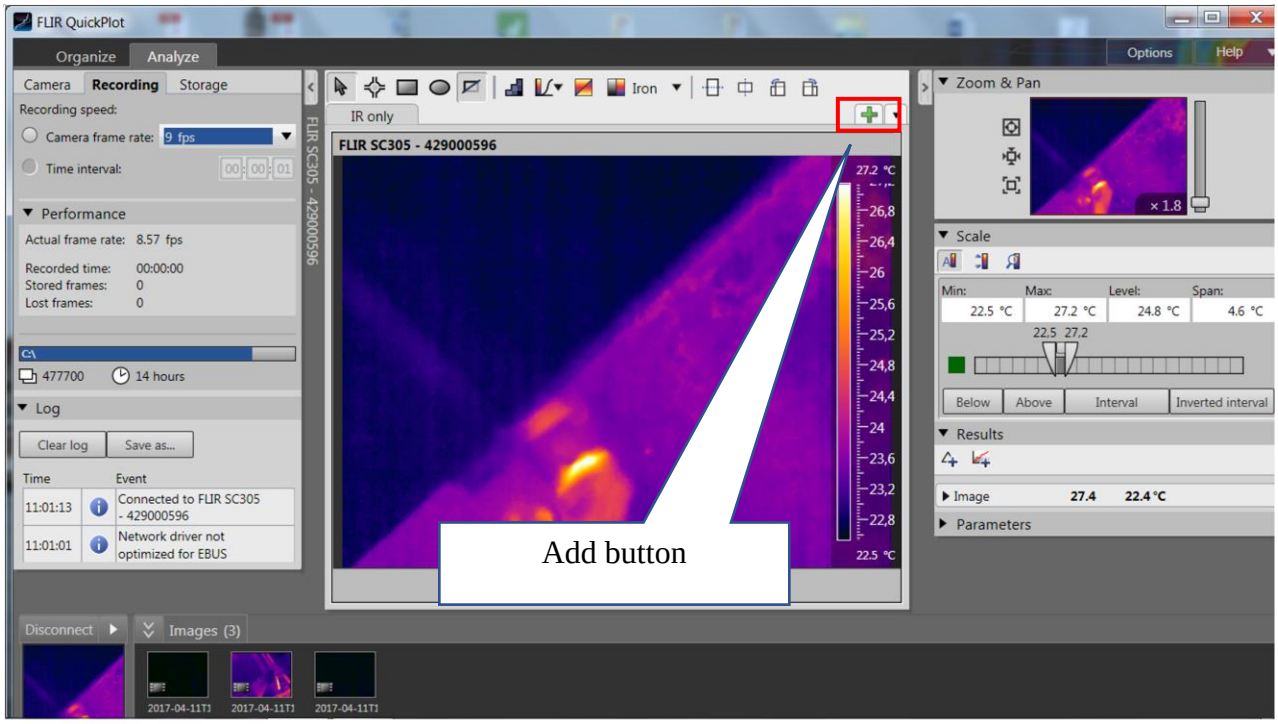

Fig III.10 e: Flir QuickPlot add button

Zoom and Panoramic controls: Contains zoom and panoramic functions to help with focusing on different sections of captured thermograms.

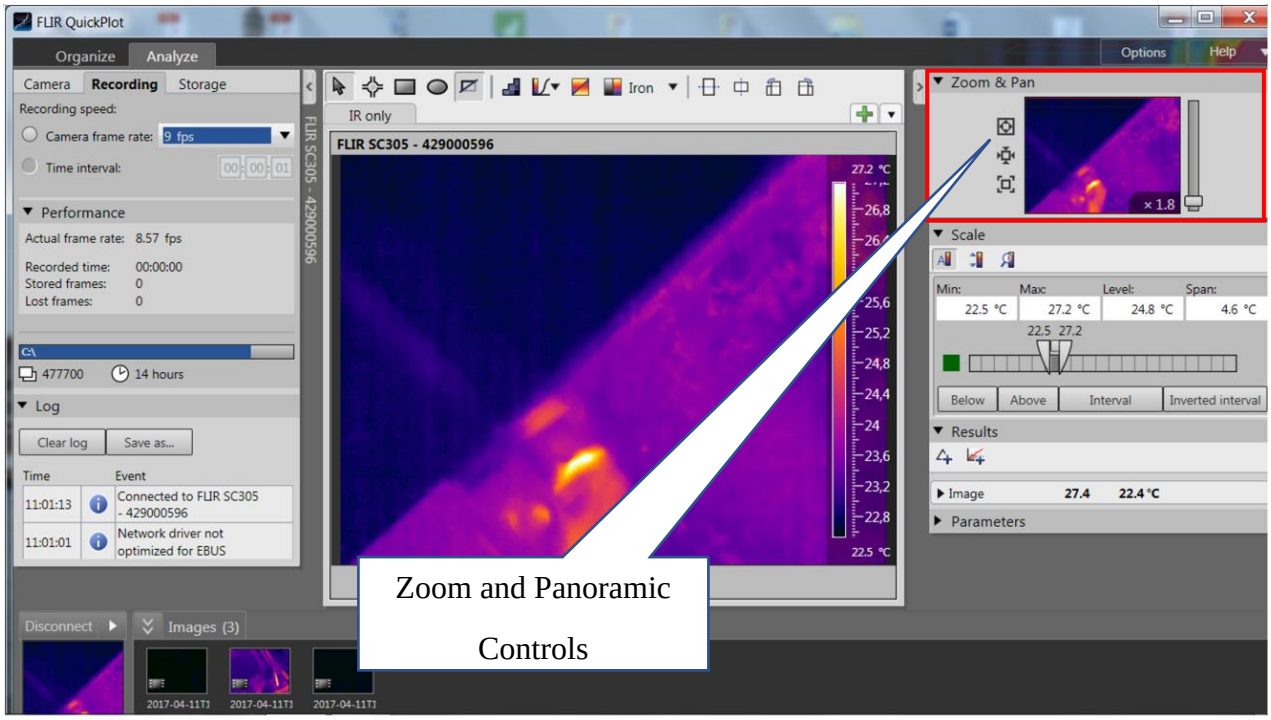

Fig III.10 f: Flir QuickPlot zoom and panoramic control

Scale control: This dropdown menu allows us to perform different adjustments on the image such as selecting a colour to represent all temperatures above or below a specific range.

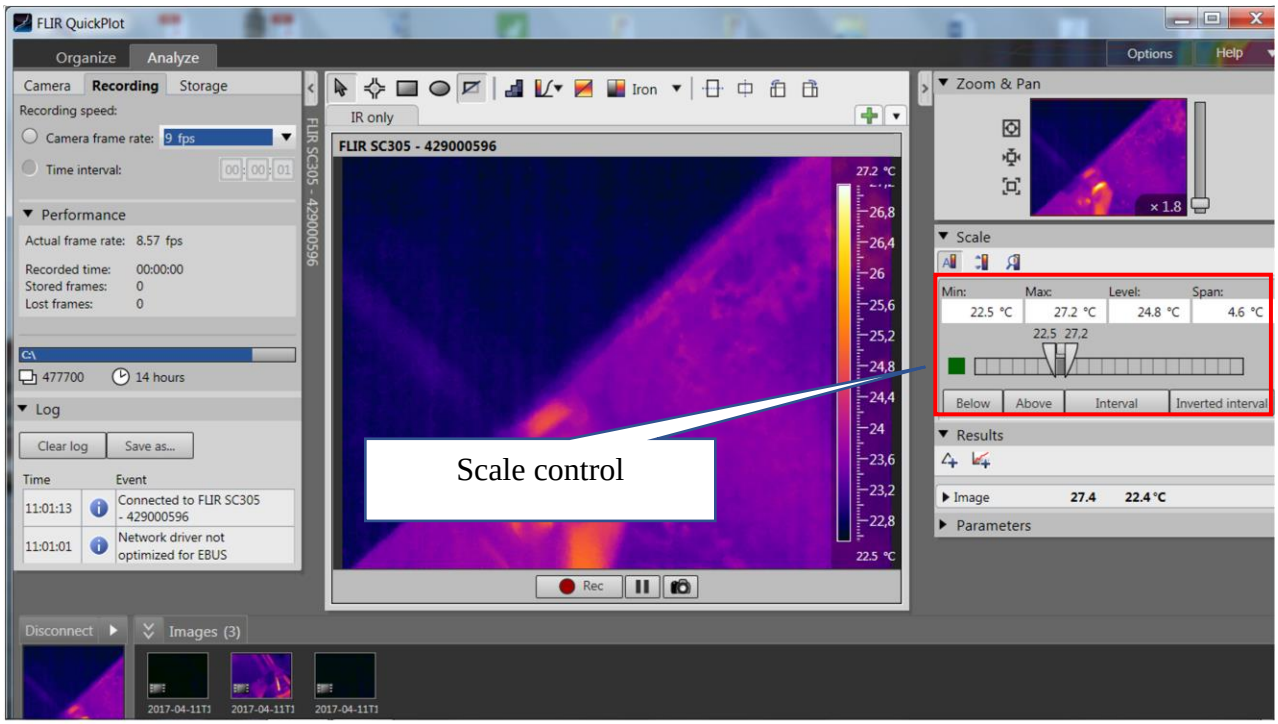

Fig III.10 g: Flir QuickPlot scale controls menu

Results dropdown menu: This dropdown serves to show the results from the selected tools on the toolbar. It also enables us to trace temperature curves.

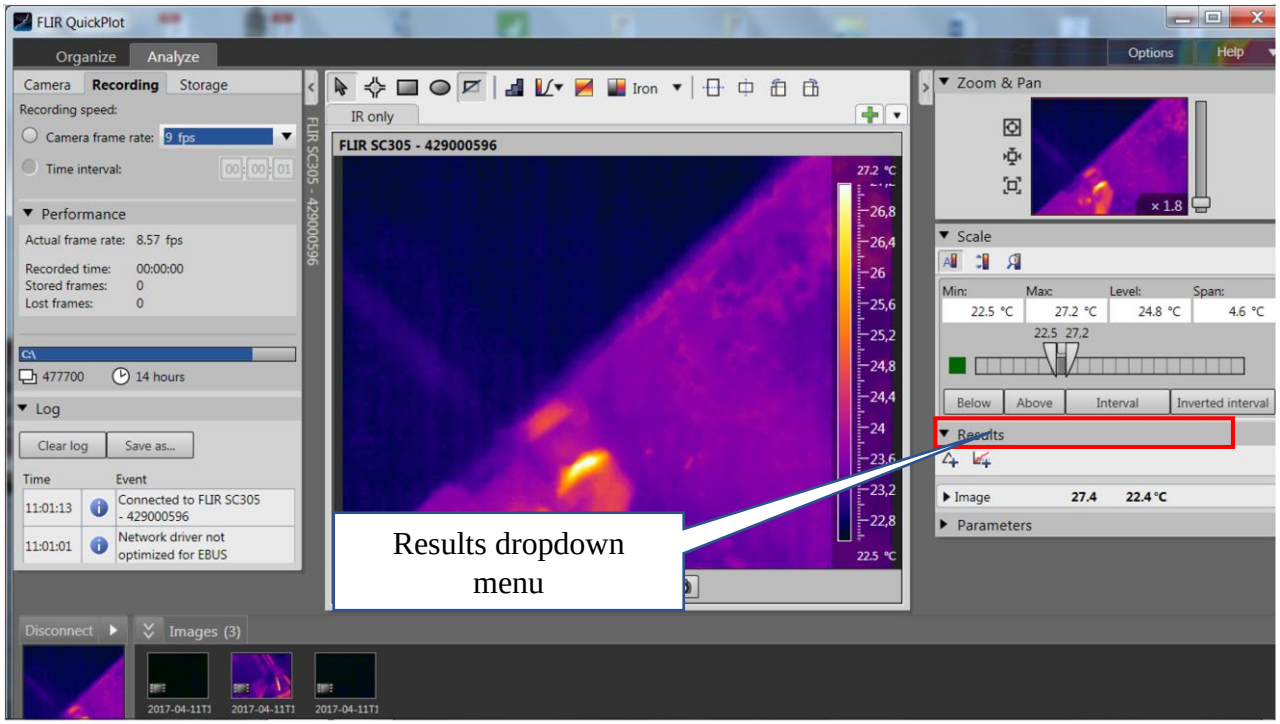

Fig III.10 h: Flir QuickPlot results dropdown menu

Live source control: Shows the name of the camera connected, as well as a live image from that specific camera.

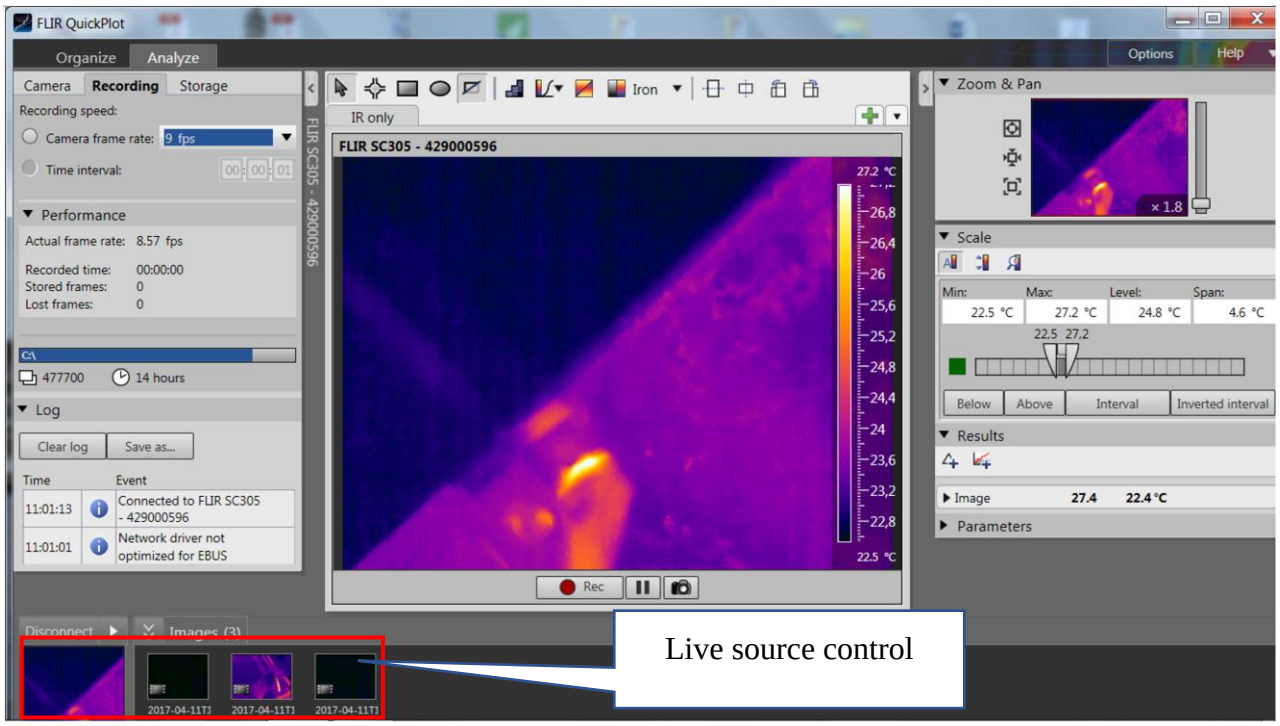

Fig III.10 i: Flir QuickPlot live source control

Connect/Disconnect button: Allow us to Connect and disconnect different cameras linked to the Flir QuickPlot software. It allows us to choose the specific camera whose signal we want to be shown.

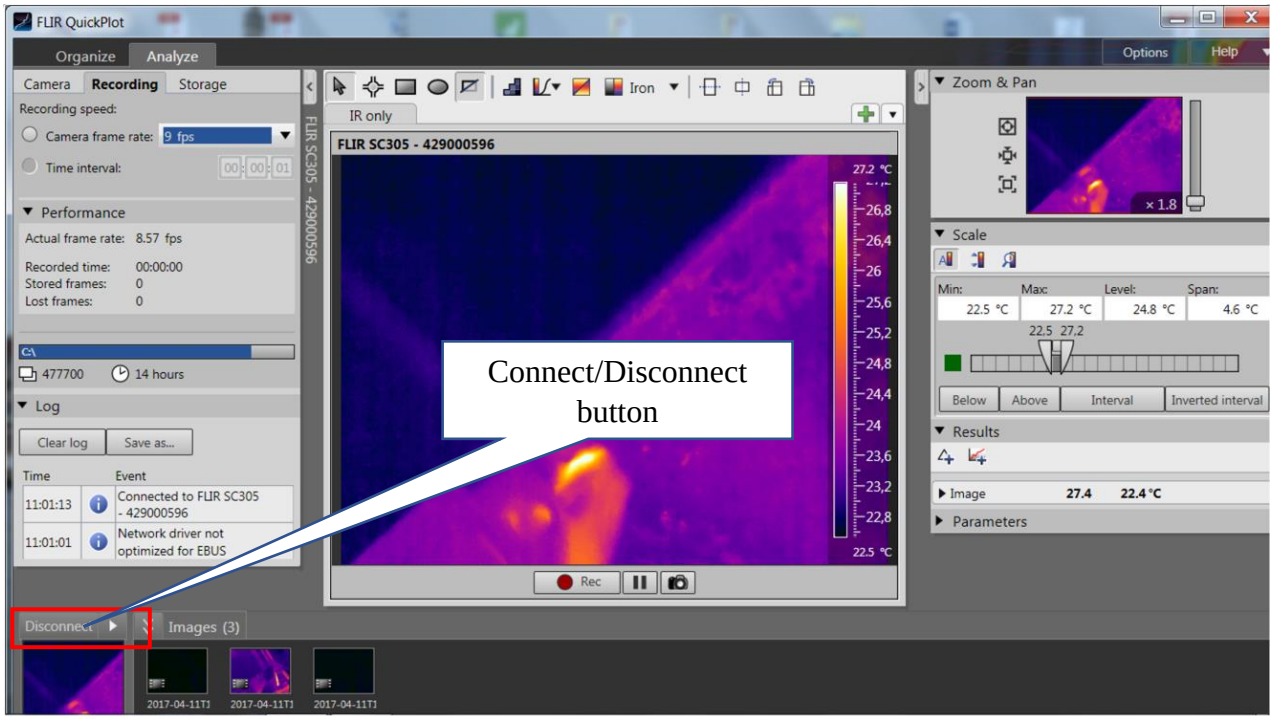

Fig III.10 j: Flir QuickPlot connect/disconnect button

Log dropdown menu: Contains information about the usage of the connected camera, this dropdown allows us to export this data in HTML or XML formats.

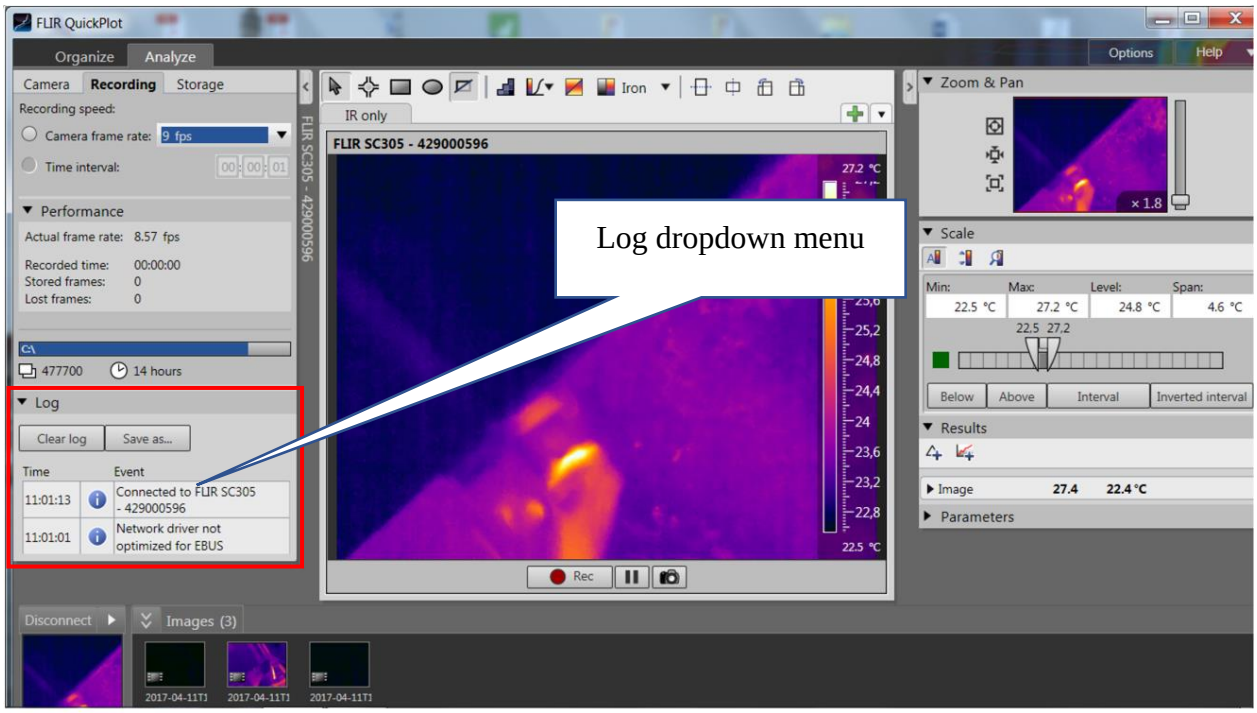

Fig III.10 k: Flir QuickPlot log dropdown menu

Performance information

This dropdown allows us to see the performance of the camera.

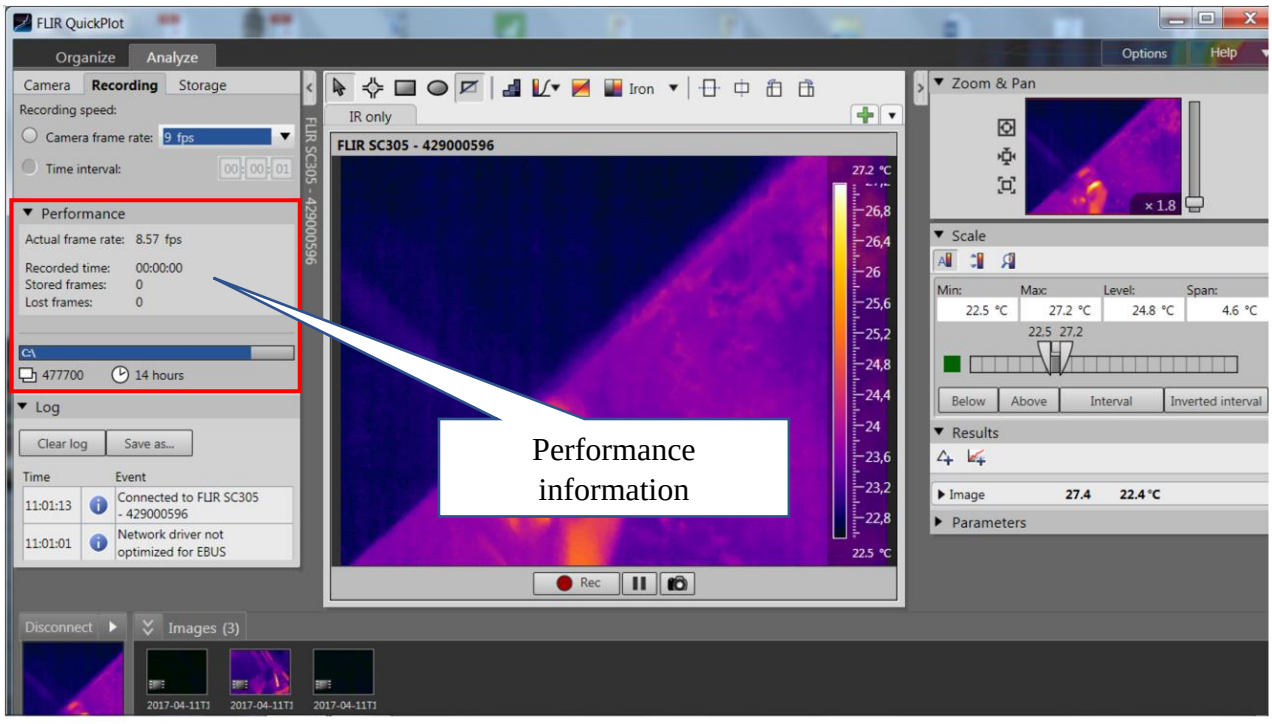

Fig III.10 l: Flir QuickPlot perfomance information dropdown menu

Recording tab: Allows us to set up image recording parameters such as the frame rate.

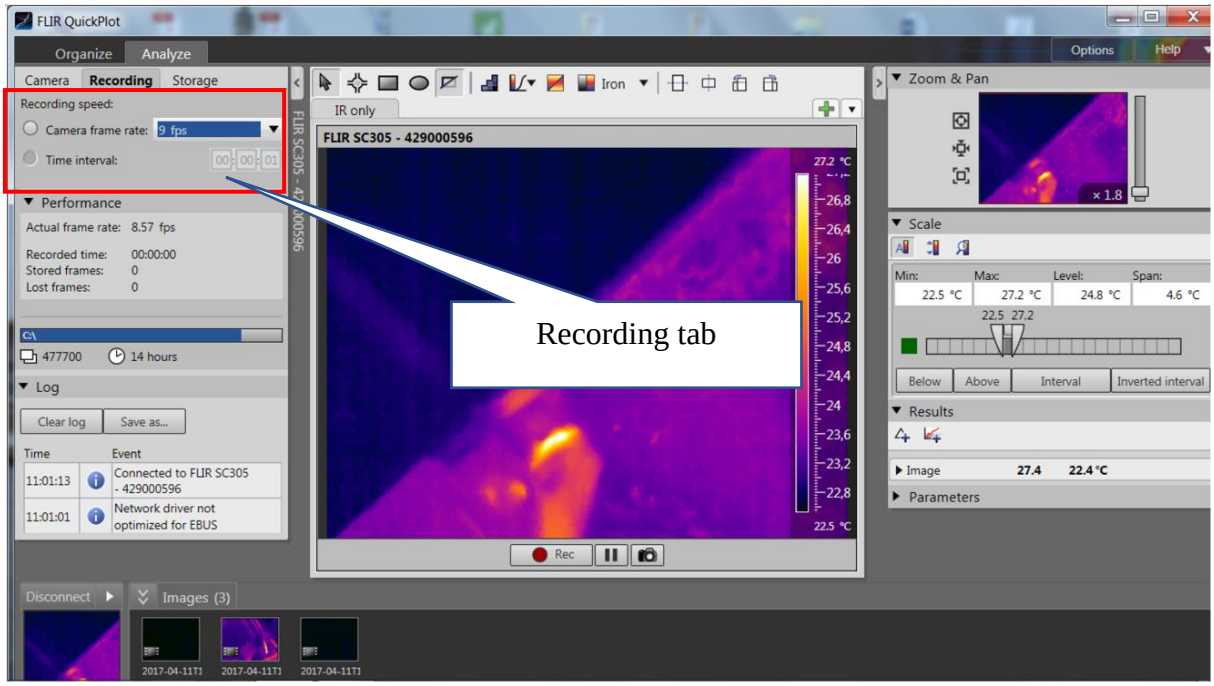

Fig III.10 m: Flir QuickPlot Recording tab

III.2.5 Experimental procedure

To perform the experiment, we followed the following steps:

- **Mounting the part**
- **Aligning the tool with the centre.**

Fig III.11: Aligning the tool with the centre.

- **Mounting the camera and adjusting the distance between the lens and the tool.**

Fig III.12: Camera mounted in front of the cutting tool.

- **Linking PC to the camera**

Fig III.13: Camera signal displayed on computer monitor.

- **Adjusting the recording settings**

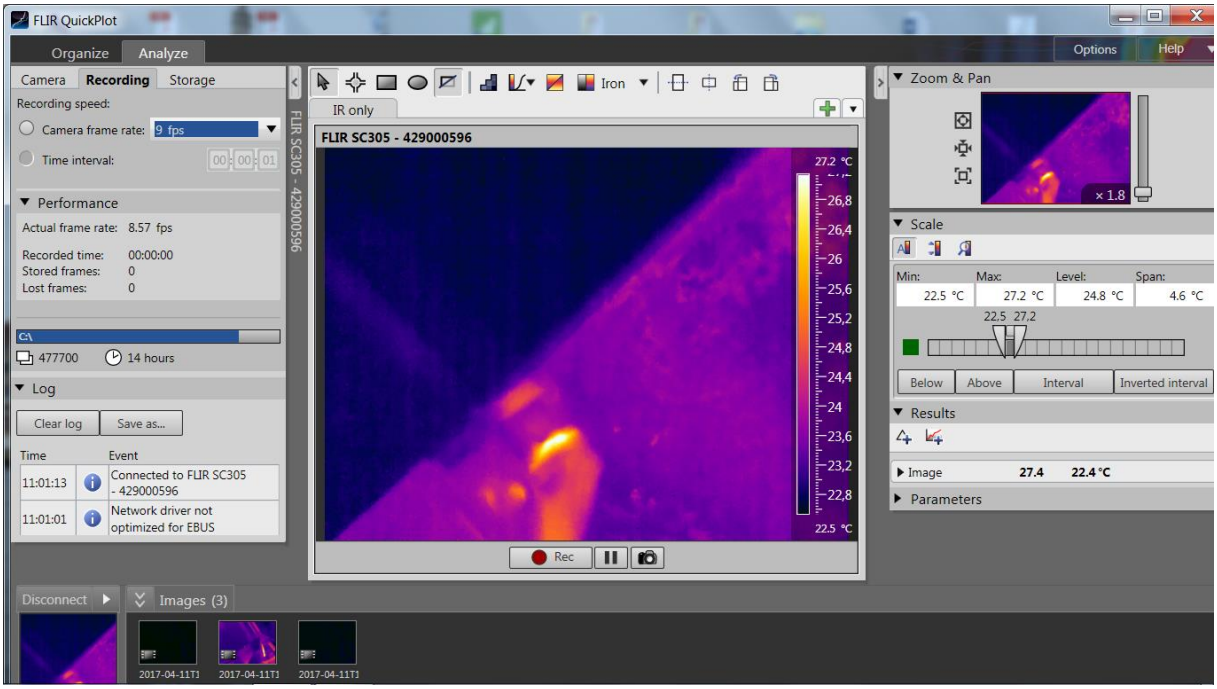

Fig. III.14: Setting the temperature range and frame rate

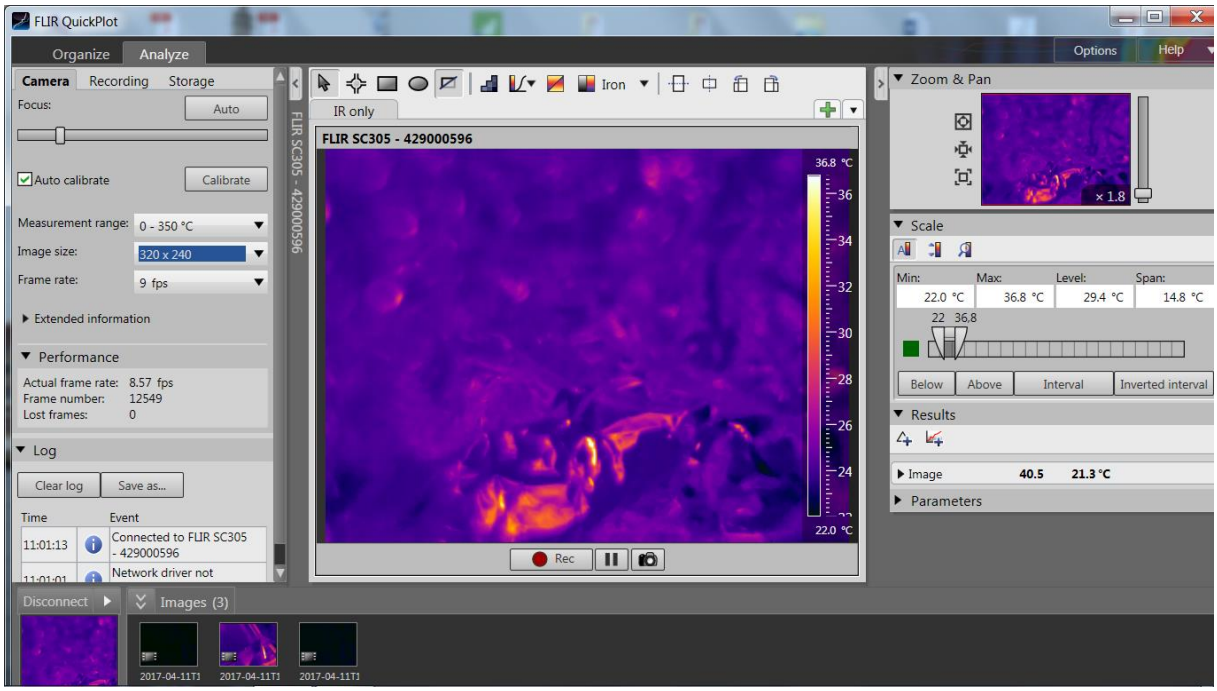

Fig III.15: Measuring the ambient temperature

- **Adjusting rotation and feed speed**

After these steps, we start the lathe to begin the machining process.

Once the lathe has started, we begin recording the machining process with the help of Flir Quickstep software until the machining process is done.

Fig III.16: Machining process image.

The next step is to save and treat the image sequence we recorded. We carried out several experiments with the workpiece. The specimen is mounted on the lathe. After adjusting the cutting parameters, a facing operation was carried out using automatic transverse movement without lubrication. The machining sequence is filmed and saved automatically by the software provided with the camera.

III.3 Expreriments

Table III.2: Table of levels.

Parameters	**Symbol**	**Level**			
		1	2	3	4
Cutting speed (Vc)	X1	78	112	157	220
Feed rate (a)	X2	0.1	0.2		
Conditions for cutting operations	The experiments were performed with no cooling or lubrification				

Since there are two variables influencing the outcome, the process can be represented using mathematical models. The mathematical models can be created using only independent variables. To do that, we can perform a statistical analysis of the results in Minitab. With Minitab, we can analyse the effect of each factor to the measured response. Which, in this case is cutting temperature. In our case, we used the cutting speed and feed rate as out determining factors.

The mathematical models are represented with the equation below:

$$\mathbf{T = f\,(v_c, a)}$$

In this case T is the cutting temperature, **a** and $\mathbf{v_c}$ are cutting velocity and feed rate respectively.

To optimize the number of experiments we do, we used the we used Minitab to generate us an optimum experimental plan. As shown in table III.2, we use the cutting speed and feed rate as two factors. Each with four and two levels respectively. Levels represent the number of values that belong to each factor.We found the optimal number of experiments to use was **eight**. Each experiment has unique combinations of factors as shown in table III.3.

Table III.3: Experimental results.

TP	Cutting conditions			Cutting temperature
	N (tr/min)	Vc(m/s)	a(mm/tr)	T(°C)
1	1000	157	0,2	203,9
2	500	78	0,1	145
3	1400	220	0,2	254,3
4	500	78	0,2	149
5	710	112	0,2	194,8
6	1400	220	0,1	212,2
7	1000	157	0,1	200,3
8	710	112	0,1	187,3

Experimental results are presented in **table III.3**. The resulting temperature from various combination of values of factors are presented in the T°C max column. This is the maximum temperature of the tool's cutting edge recorded for each experiment. The temperature ranges from 145 degrees Celsius to 254.3 degrees Celsius.

We can use the experimental results to construct a first order mathematical model with the following format:

$$Y = a_0 + a_1 X_1 + ... + a_k X_k$$

The least squares method can be used to find constants. Adopting the equation III.2 to our study, it becomes:

$$T = b_0 + b_1 X_1 + ... + b_k X_k$$

Where T=Y which is the response (cutting temperature) based on the first order equation.

$X_1 X_2 \ldots X_k$ are factors of control, which in our case are (cutting speed and feed rate). $b_0, b_1 ... b_k$ are constants to be determined using the least squares method.

Conclusion

Infrared thermography has numerous advantages that include measuring temperature at a distance and real time temperature surveillance. The measurement can be done with little to no loss of temperature to the environment. To obtain an optimal number of experiments, we employed the experimental planning methos, where we found the number of experiments to run to be 8. We also recorded the results that will be useful for the for creating a mathematical model in the following chapter.

CHAPTER IV: **Results and discussion**

IV.1 Introduction

Prior to analysing the results, we extracted the data from the camera's software (FLIR Quick Plot) in order to visualize the machining sequences.

We carried out the following operations:

1. Importation of the machining sequence (test).

2. Define the measurement area.

3. Introducing the thermal scene's parameters (reflection, distance, atmospheric temperature, emissivity, etc.).

4. Selecting a scale to ensure a good sequence visualization.

5. Establish the colour scheme.

6. Sequence visualization.

7. Tracing the curve of temperature as a function of time.

8. Making the chosen zone's temperature table for use in our analysis.

IV.2 Experimental analysis

The experiences conducted are based on the experimental design table with experiments. The purpose of both the analysis of variance and regression analysis is to examine the impact of the cutting parameters on temperature. We also used Minitab V21.2, a statistical and experiment planning tool, to analyse the effects of the cutting conditions on temperature and to exploit experimental and predicted results. Throughout this work, we have employed a second-order equation for temperature prediction based on cutting conditions. The experimental results are shown in **Table III.3.**

The next section of this chapter will show experimental results classified in order from the highest to the lowest maximum cutting temperature.

The curve with the highest maximum temperarue(254.3ºC) is that of the third experiment. The parameters for the third experiment were turning speed, N=1400tr/min and advance speed, a=0.2mm/tr.

Table IV.1: Experimental results of experiment 3

TP	N(tr/min)	a(mm/tr)	Vc(m/min)	TºC
3	1400	0,2	220	254,3

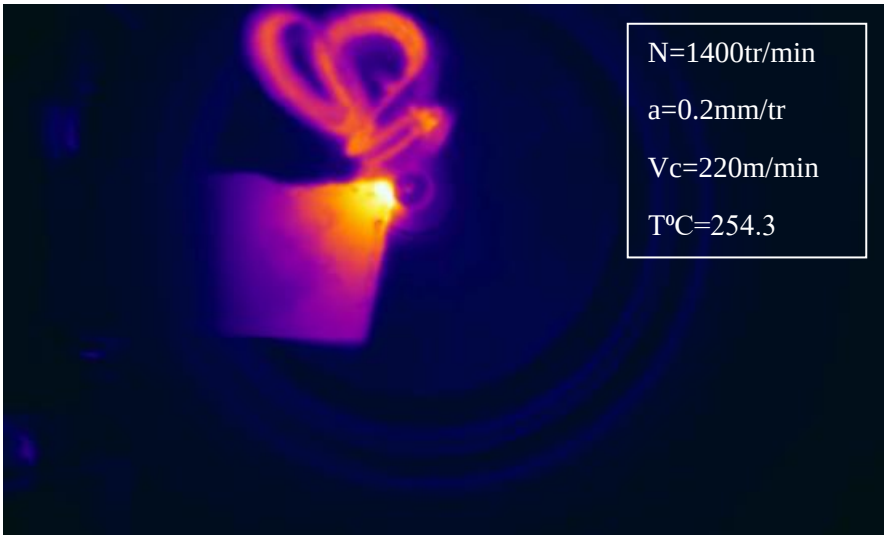

(a)

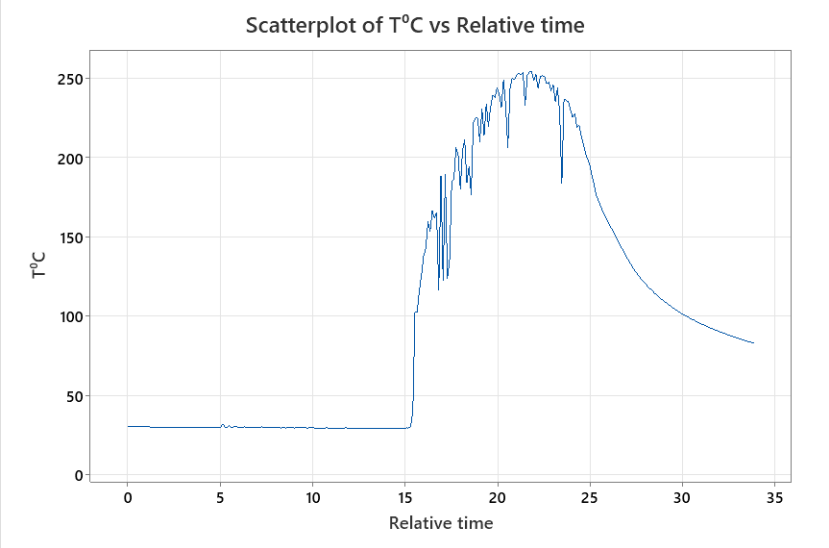

(b)

Fig. IV.1: (a) Experiment 3 thermogram and **(b)** evolution of temperature with time.

The curve with the second highest maximum temperarue(212.2ºC) is that of the sixth experiment. The parameters for the sixth ecperiment were turning speed, N=1400tr/min and advance speed, a=0.1mm/tr.

Table IV.2: Experimental results of experiment 6

TP	N(tr/min)	a(mm/tr)	Vc(m/min)	Tº C
6	1400	0,1	220	212,2

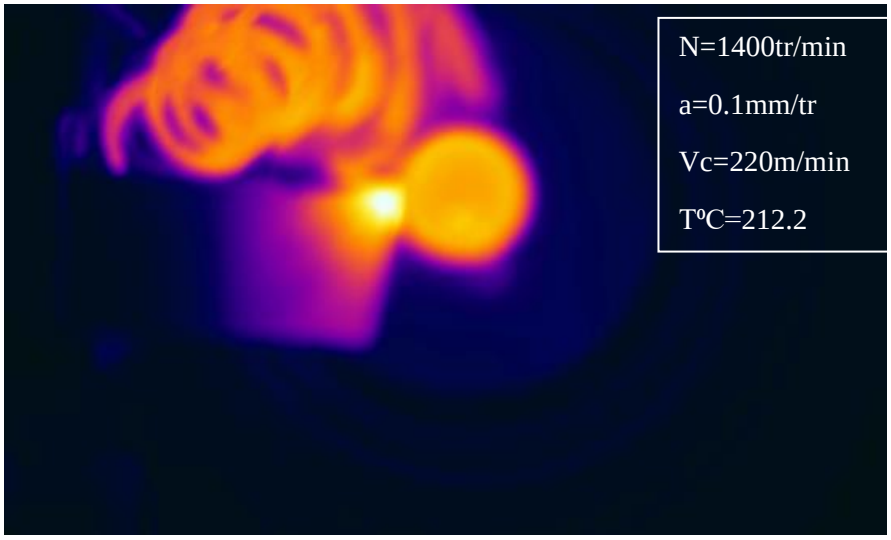

(a)

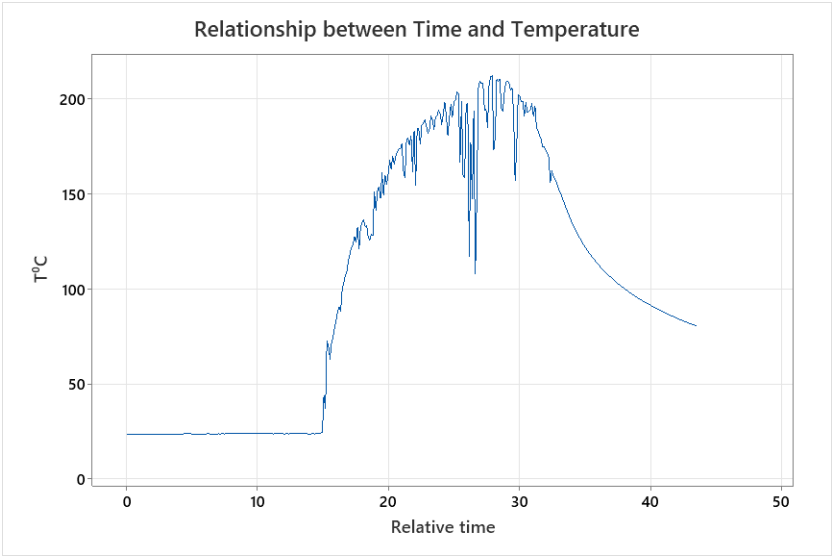

(b)

Fig. IV.2: (a) Experiment 6 thermogram and **(b)** evolution of temperature with time.

The curve with the third highest maximum temperarue(203.9ºC) is that of the first experiment. The parameters for the first ecperiment were turning speed, N=1000tr/min and advance speed, a=0.2mm/tr.

Table IV.3: Experimental results of experiment 1

TP	N(tr/min)	a(mm/tr)	Vc(m/min)	TºC
1	1000	0,2	157	203,9

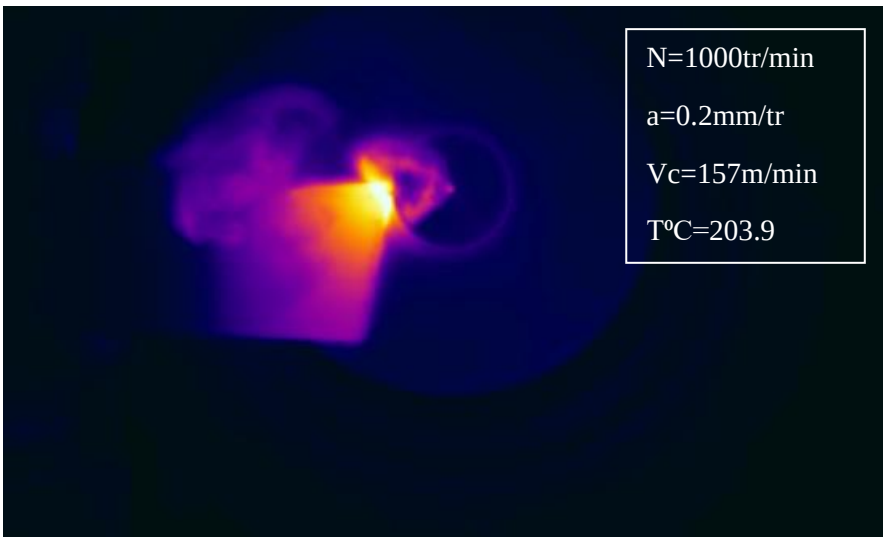

(a)

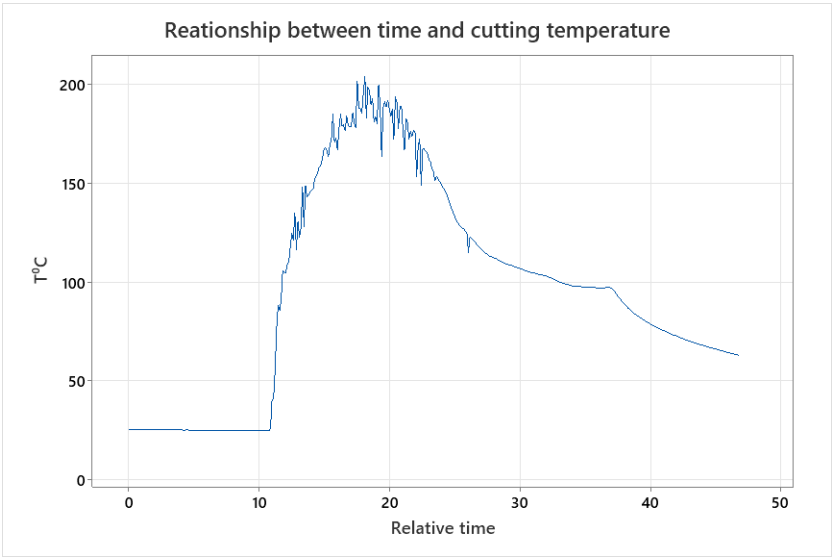

(b)

Fig. IV.3: (a) Experiment 1 thermogram and **(b)** evolution of temperature with time.

The curve with the fourth highest maximum temperarue(200.3ºC) is that of the seventh experiment. The parameters for the seventh ecperiment were turning speed, N=1000tr/min and advance speed, a=0.1mm/tr.

Table IV.4: Experimental results of experiment 7

TP	N(tr/min)	a(mm/tr)	Vc(m/min)	TºC
7	1000	0,1	157	200,3

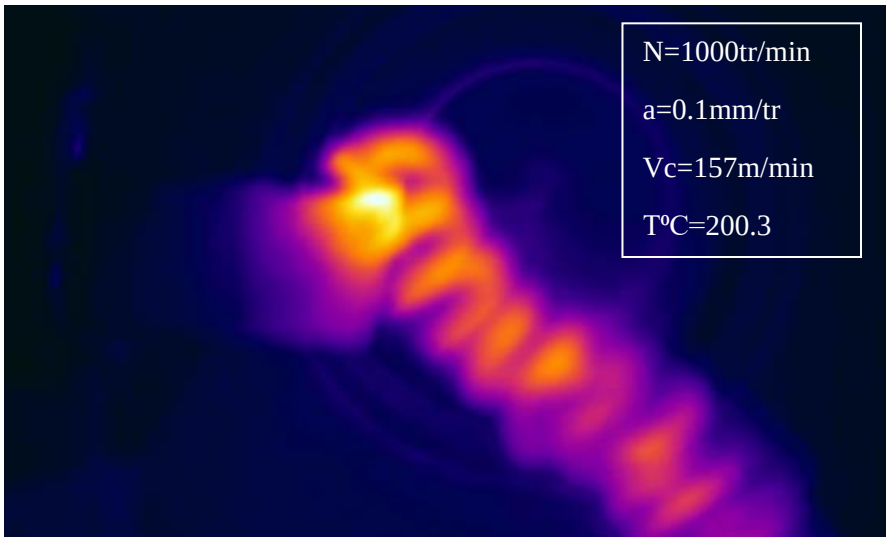

(a)

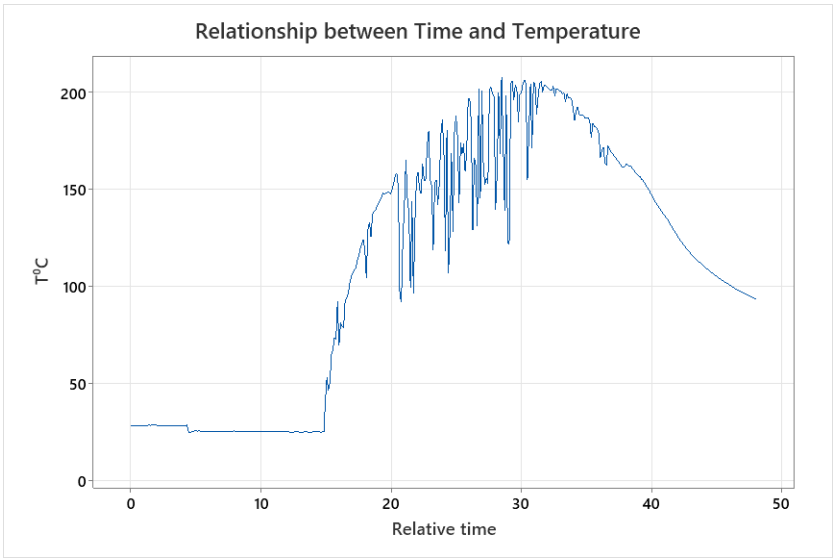

(b)

Fig. IV.4: (a) Experiment 7 thermogram and **(b)** evolution of temperature with time.

The curve with the fifth highest maximum temperarue(194.8ºC) is that of the fifth experiment. The parameters for the fifth ecperiment were turning speed, N=710tr/min and advance speed, a=0.2mm/tr.

Table IV.5: Experimental results of experiment 5

TP	N(tr/min)	a(mm/tr)	Vc(m/min)	TºC
5	710	0,2	112	194,8

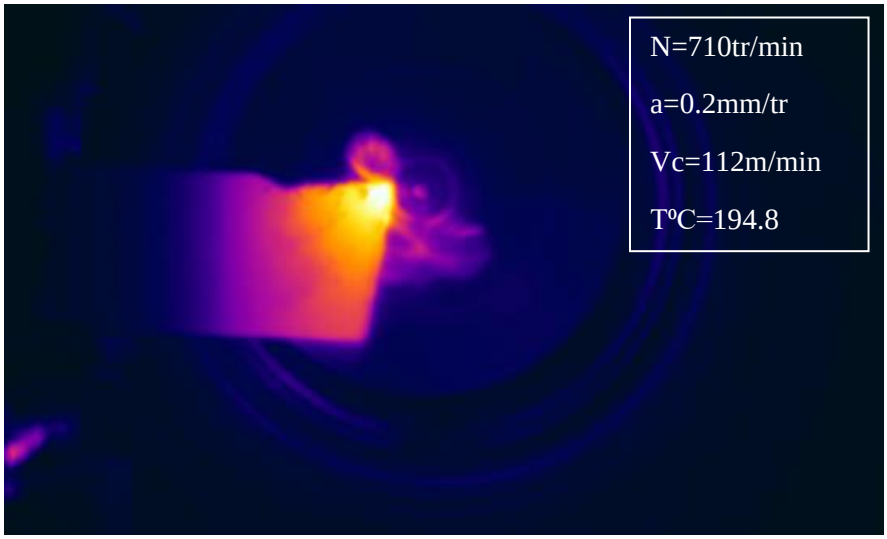

(a)

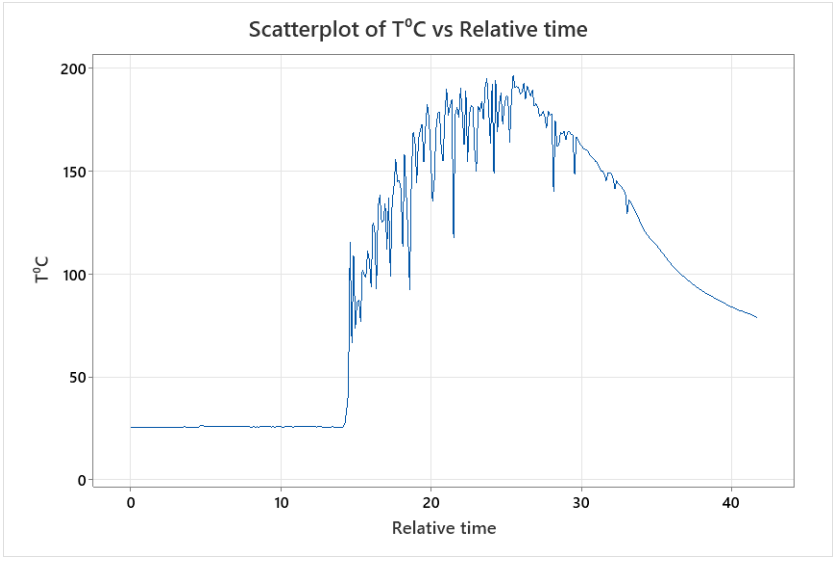

(b)

Fig. IV.5: (a) Experiment 5 thermogram and **(b)** evolution of temperature with time.

The curve with the sixth highest maximum temperarue(187.3ºC) is that of the eighth experiment. The parameters for the eighth ecperiment were turning speed, N=710tr/min and advance speed, a=0.1mm/tr.

Table IV.6: Experimental results of experiment 8

TP	N(tr/min)	a(mm/tr)	Vc(m/min)	TºC
8	710	0,1	112	187,3

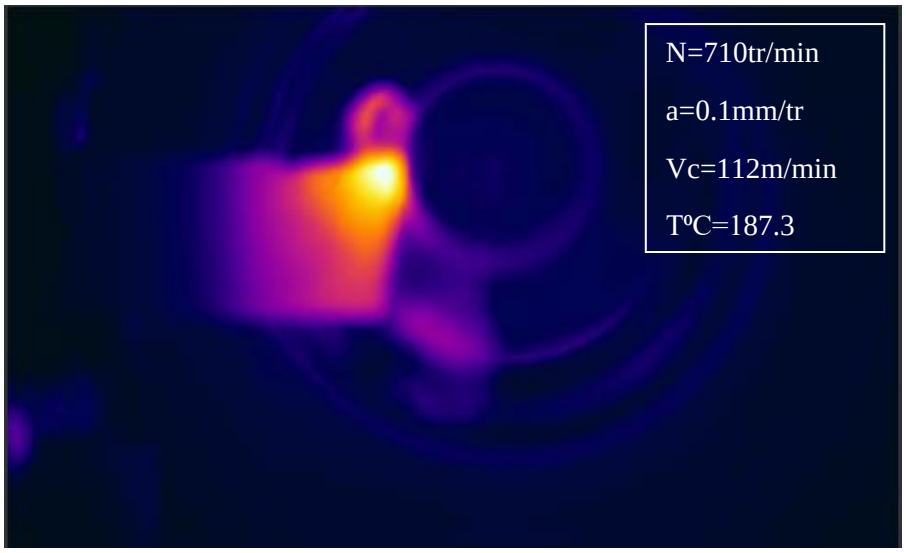

(a)

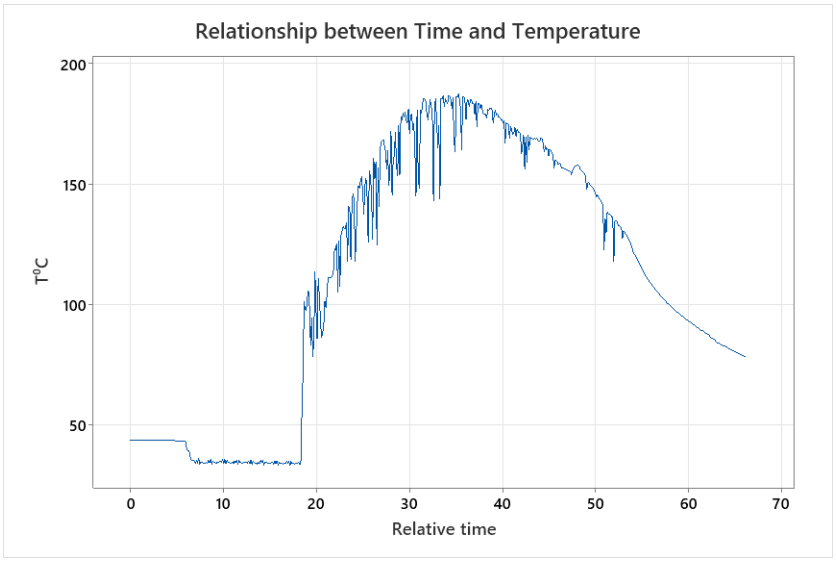

(b)

Fig. IV.6: (a) Experiment 8 thermogram and **(b)** evolution of temperature with time.

The curve with the seventh highest maximum temperarue(149ºC) is that of the fourth experiment. The parameters for the fourth ecperiment were turning speed, N=500tr/min and advance speed, a=0.2mm/tr.

Table IV.7: Experimental results of experiment 4

TP	N(tr/min)	a(mm/tr)	Vc(m/min)	TºC
4	500	0,2	78	149

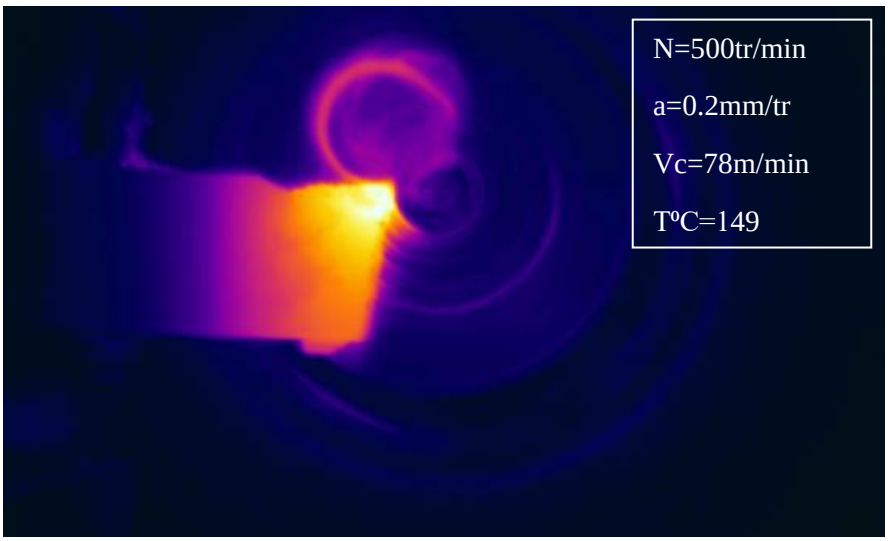

(**a**)

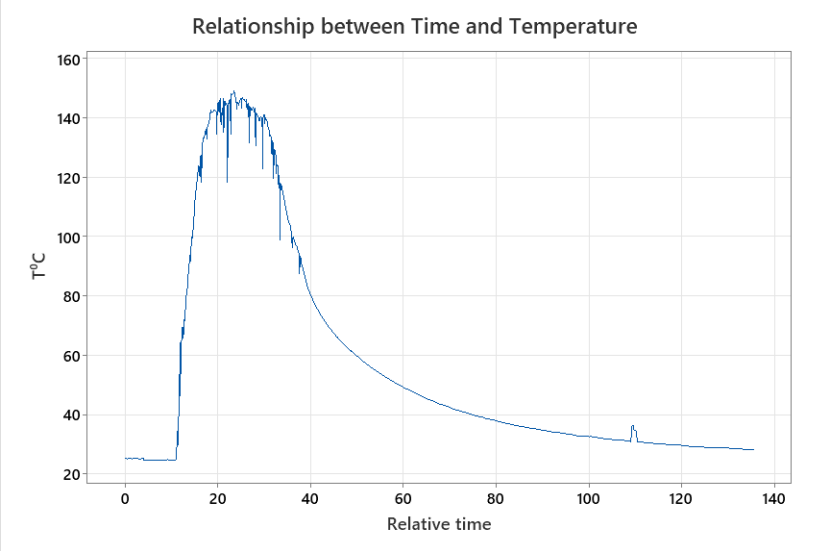

(b)

Fig. IV.7: (a) Experiment 4 thermogram and **(b)** evolution of temperature with time.

The curve with the eighth highest maximum temperarue(145ºC) is that of the second experiment. The parameters for the second ecperiment were turning speed, N=500tr/min and advance speed, a=0.1mm/tr.**Table IV.2**: Experimental results of experiment 6

Table IV.8: Experimental results of experiment 2

TP	N(tr/min)	a(mm/tr)	Vc(m/min)	TºC
2	500	0,1	78	145

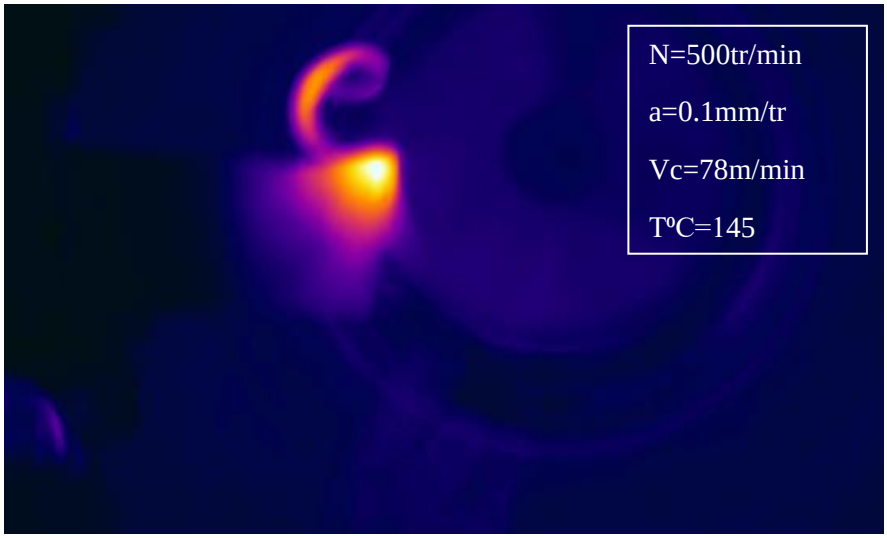

(a)

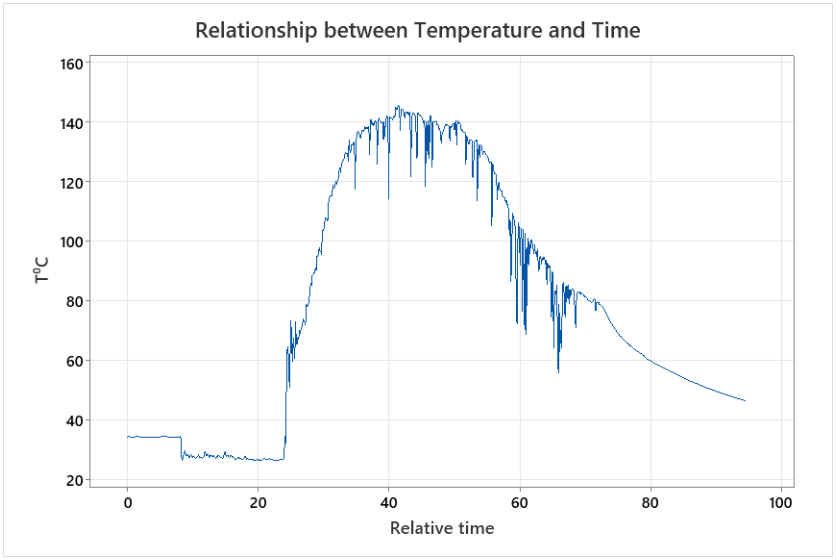

(b)

Fig. IV.8: (a) Experiment 2 thermogram and **(b)** evolution of temperature with time.

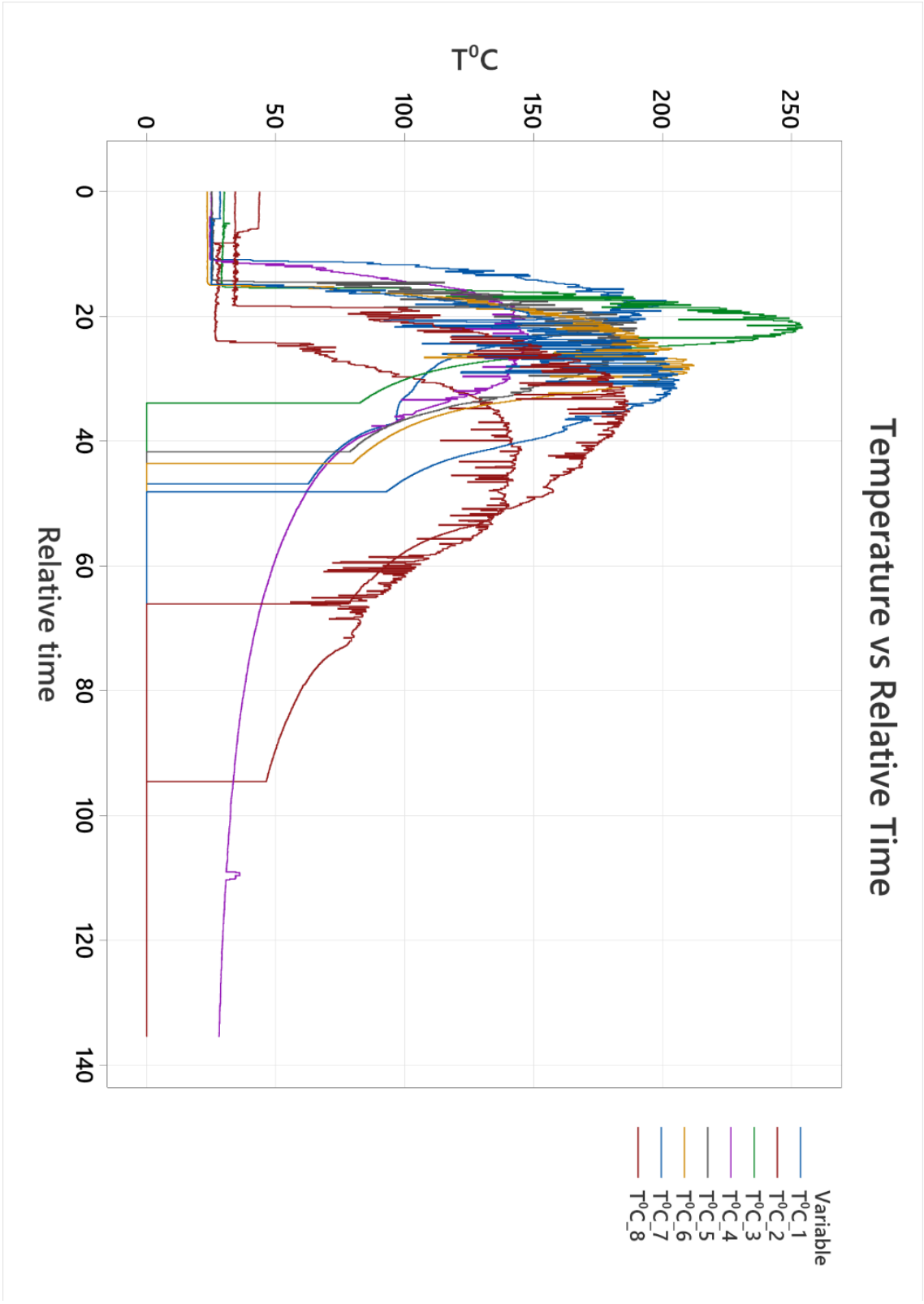

Fig. IV.9: Superimposed graphs of temperature in function of relative

Fig. IV.9 shows the superimposed graphs from all experimental results. From the superimposed curves, we notice that the shape of the different curves is similar. We see that the cutting temperature rapidly increases until it reaches the maximum point for each curve (approximately as cutting tool approaches the halfway through the radius). From then, the cutting temperature gradually decreases as the tool approaches the centre of the workpiece and hence the cutting speed decreases. **Fig. IV.9** illustrates this phenomenon

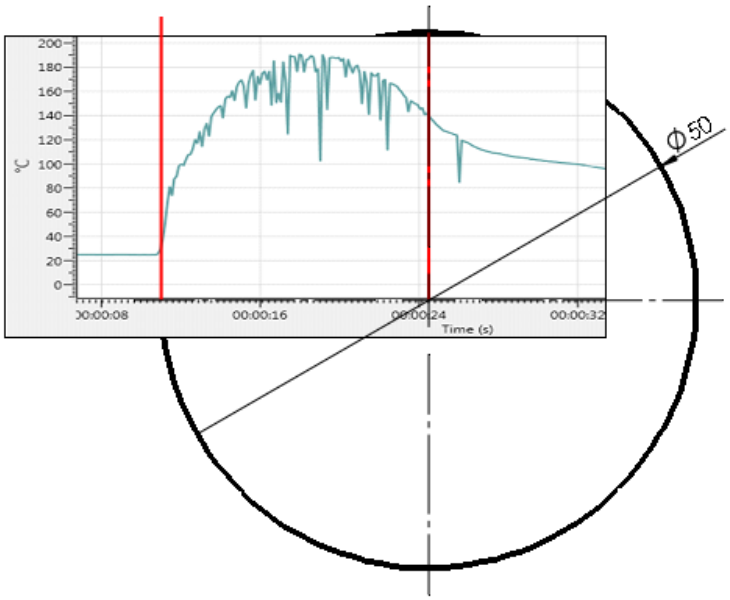

Fig. IV.10: Variation of temperature with the radius of the workpiece

Fig. IV.10 shows how the temperature changes during an orthogonal drilling operation. As the tool gets closer to the centre, the temperature rises; notice that the temperature reaches its maximum at 1/2 of the piece's radius (187°C).

IV.3 Statistical study

IV.3.1 Temperature prediction model

The cutting temperature can be predicted using a mathematical model created from the experimental results in **Table III.3.**

Table IV.9: Coefficients of the regression equation

Term	Coe	SE Coef	T-Value	P-Value	VIF
Constant	126.5	59.6	2,12	0,124	
N	0.119	0.105	1,13	0,342	66,83
a	-425	276	-1,54	0,221	8,14
Nx**N**	-0.000057	0.000049	-1,16	0,329	54,97
Nx**a**	0.545	0,286	1,90	0,153	20,01

The regression equation is a second order equation that can be written in the following way:

$$\mathbf{T° = 126{,}5 + 0{,}119 \times N - 425 \times a - 0{,}000057\ N^2 + 0{,}545\ N \times a} \qquad (°C)$$

IV.3.2 Precision of the model and the error between predicted and experimental temperature

To calculate the percentage error of the 8 experiments, we use the following formula:

$$e_i = \left[\frac{|T_{exp} - T_{pred}|}{T_{exp}}\right] \times 100 \qquad (\%)$$

T_{exp}: Experimental temperature

T_{pred}: Predicted temperature

e_i: Percentage error

To calculate the precision percentage, we use the following formula:

$$A_i = \frac{1}{n}\sum_{i=0}^{n}\left[1 - \frac{|T_{exp} - T_{pred}|}{T_{exp}}\right] \times 100 \qquad (\%)$$

n: Number of experiments (*n*=8)

A: Precision

Table IV.10 shows the error and precision for each experiment as the values are compared to values predicted by equation IV.1

Table IV.10: Comparison between predicted and recorded values

TP	Cutting conditions			Cutting temperature		Error%	Precison%
	N (tr/min)	Vc(m/s)	a(mm/tr)	$T(^0C)_{exp}$	$T(^0C)_{pred}$		
1	1000	157	0,2	203,9	212,50	4,22	95,78
2	500	78	0,1	145	156,50	7,93	92,07
3	1400	220	0,2	254,3	248,98	2,09	97,91
4	500	78	0,2	149	141,25	5,20	94,80
5	710	112	0,2	194,8	174,65	10,35	89,65
6	1400	220	0,1	212,2	215,18	1,40	98,60
7	1000	157	0,1	200,3	200,50	0,10	99,90
8	710	112	0,1	187,3	178,45	4,72	95,28

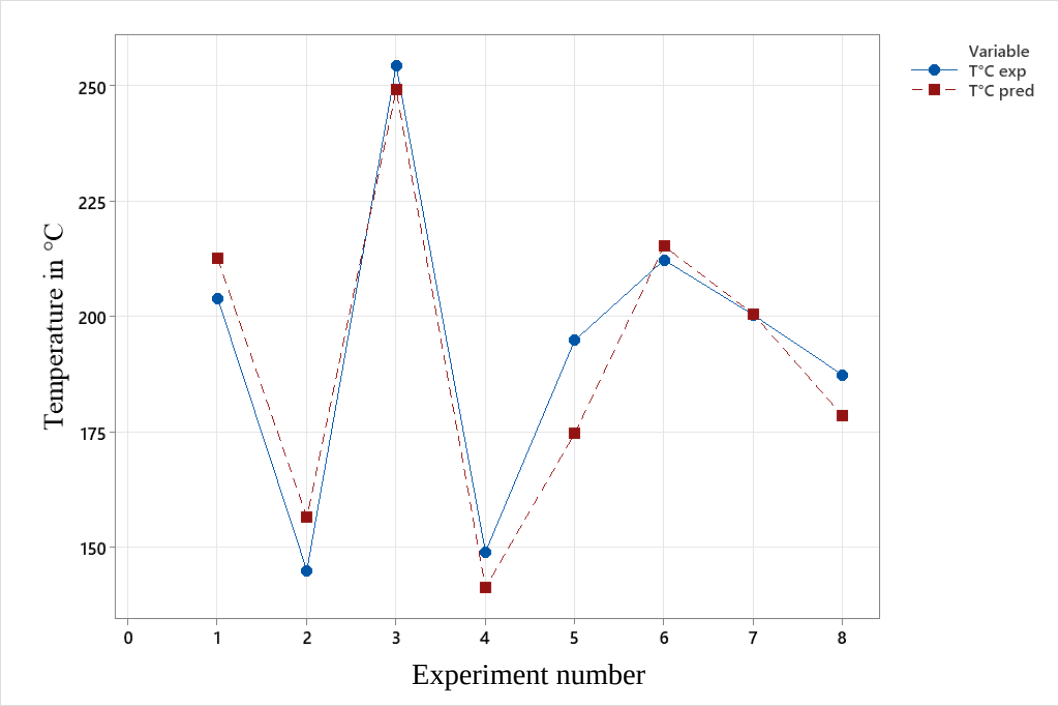

Fig. IV.11: Comparison between experimental and predicted values for cutting temperature.

The figure illustrates how the estimated values and experimental values are within **95.50%** precision. Essentially, these outcomes demonstrate the accuracy of the model.

Furthermore, the results validate that the model can be used effectively with a **95.50%** confidence interval to predict the temperature for usage.

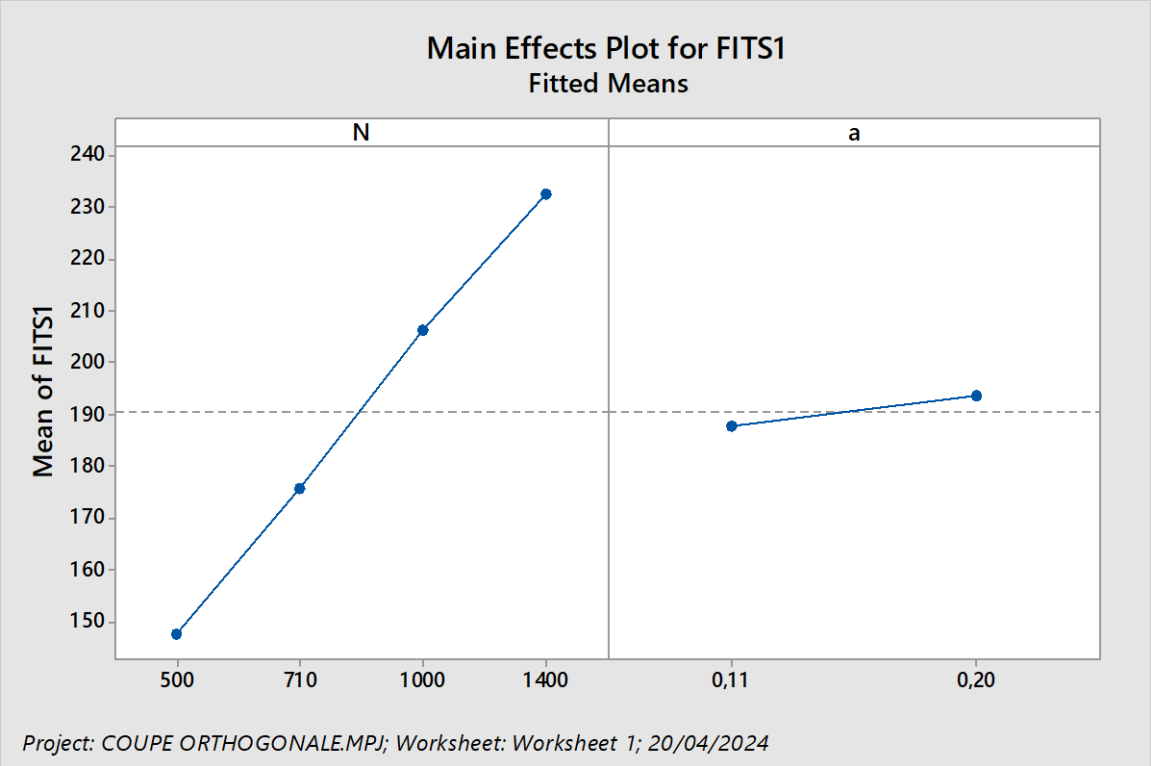

Fig. IV.12: Effects of Cutting Conditions on Cutting Tool Temperature

The figure illustrates the impact of the cutting conditions, namely rotation frequency and advance, on temperature variation. It is evident that the rotation frequency has a net positive impact on temperature rise while having a negligible effect on temperature advance. The analysis of the residual distribution is based on a test that looks for non-normality. Figure V-2 displays the normal probability trace. It is evident that the residuals are located close to the reference line, indicating a normal distribution of errors.

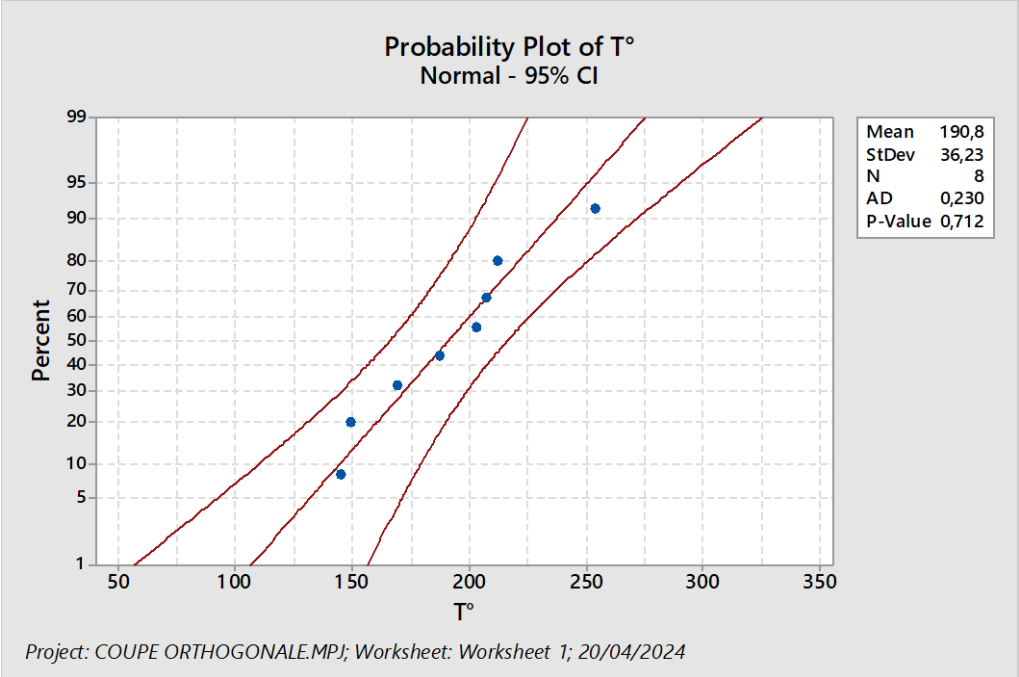

Fig. IV.13: Normality line of the distribution of residues.

IV.3.3 Analysis of Variance

Minitab **V21.2** software is used to perform the analysis of variance (ANOVA) using the method of least squares. The results of this statistical technique are displayed in Table **IV.9**. In order to assess the main effects of the factors on the studied responses, the analysis table is typically based on the measured parameters.

The model's "P-value" are determined by dividing the average of the model's squares' sum by the average of the residual squares sum. Furthermore, if the "P-value" is extremely small (less than or equal to 0.05), the model's bounds will significantly affect the result.

The analysis shown in **Tableau V.3** demonstrates that, for a 95% confidence level, the temperature is significantly impacted by the cutting frequency (N) and advance (a).

Table IV.11: Variance analysis

Source	DF	Adj SS	Adj MS	F-Value	P-Value
Regression	4	8735,4	2183,9	14,43	0,027
N	1	192,4	192,4	1,27	0,342
a	1	359,3	359,3	2,37	0,221
NxN	1	204,7	204,7	1,35	0,329
N*a	1	548,1	548,1	3,62	0,153
Error	3	454,1	151,4		
Total	7	9189,5			

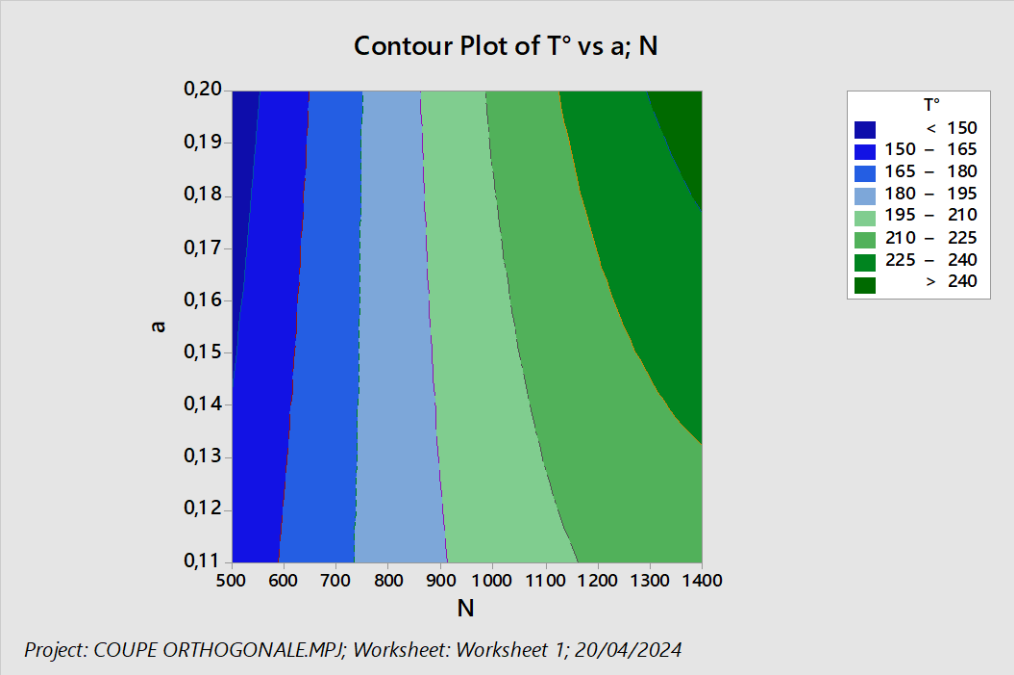

Fig. IV.14: Isotherm according to rotation frequency and feed

Fig. IV.14 displays a graph showing the comparison of the experimental and predicted values for the temperature model obtained using the surface response methodology.

This demonstrates the closeness between estimated values and experimental values. In fact, these results demonstrate the model's accuracy.

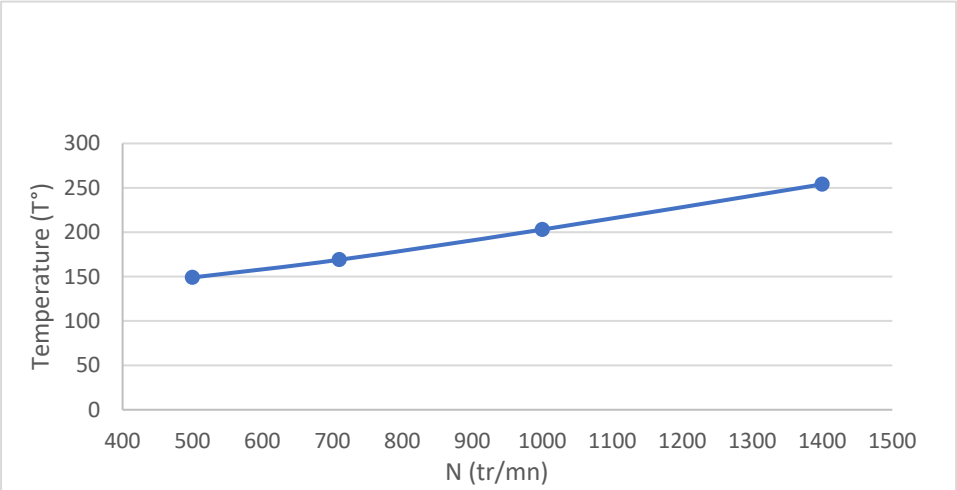

Fig. IV.15: Temperature variation as a function of rotation frequency for a=0.2mm/rt

Fig. IV.15 illustrates how temperature increases linearly for a 0.2 mm/tr feed rate in rotation frequency. In **Fig. IV.16** note that the temperature rises for frequencies between 500 tr/min and 710 tr/min, followed by a stabilization of the temperature given the small feed rate of 0.1.

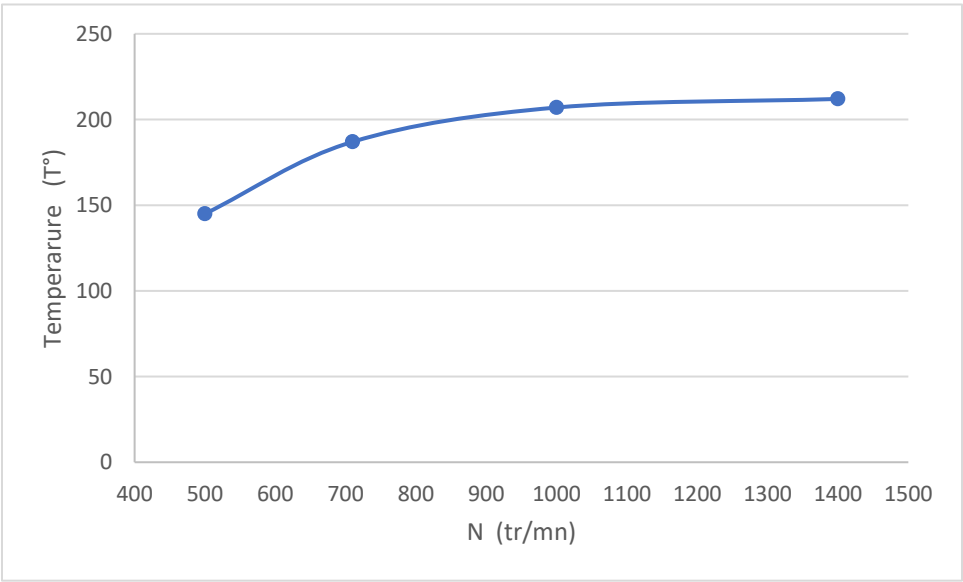

Fig. IV.16: Temperature variation as a function of rotation frequency for a=0.1mm/t

Conclusion

This study shows that thermography is a useful procedure for developing an experimental methodology that allows one to measure the cutting temperature during machining. With this experiment we were able to record the temperature of the machined surface and the cutting edge of the cutting tool. The model's accuracy has been confirmed and found to be appropriate at a precision level of 95.5% for temperature readings taken during operation demonstrating the model's potential for temperature prediction. This technique may be a cost-effective and efficient way to predict temperature and optimize the coupling parameters.

General Conclusion

The shear stress induced by the cutting tool on the workpiece causes an increase in temperature of the tool-workpiece interface. This increase in temperature had a profound influence on the type of materials used to manufacture cutting tools as well as the optimal parameters required for machining. It also has an influence on the tool's lifespan as well as the choice of a lubricant that can withstand amount of heat produced during a particular machining operation.

In this study we have presented numerous results for different cutting parameters and we have explained how different parameters affect the temperature of the tool-workpiece interface during the machining of aluminium alloy, which was recorded using an infrared camera (Flir 305sc). The advantage of using an infrared camera is that we can record temperature observations without making contact with the tool or workpiece. The method can be used with minimal heat loss to the environment. It can also be a great method for real time temperature surveillance.

To optimise the choice and combination of cutting conditions, and to find the necessary number of experiments for this study, we used the experimental design method. After analysing the experimental results, we were able to come up with a second-degree polynomial equation for the prediction of cutting temperature with an accuracy of 95.5%. Tracing experimental and predicted results on the same graph, we have noted that they look similar. This supposes that our prediction model can be reliable, which means that the cutting temperature varies with cutting conditions.

We have also noted that the factor that has the most significant influence of the cutting temperature is the rotation speed of the workpiece as shown by the analysis of the results.

Bibliographic references

[1]. Dr. BENNEGADI, Mohammed El Larbi (2018). Coupe des Métaux en Fabrication Mécanique et Productique. Cours, USTO, Oran.

[2]. Nedić, B., & Erić, M. (2014). Cutting temperature measurement and material machinability. Thermal Science, 18(suppl.1), 259–268. https://doi.org/10.2298/tsci120719003n

[3]. TEBIB, A. and ARBAOUI, M.E.H., Surveillance de la Température de Coupe Pendant le Tournage de l'Acier AISI 1060 en Utilisant la Logique Floue (Doctoral dissertation).

[4]. Groover, M.P., 2020. Fundamentals of modern manufacturing: materials, processes, and systems. John Wiley & Sons.

[5]. Blais, C., 2000. Contributions à l'amélioration de l'usinabilité de pièces fabriquées par métallurgie des poudres. École Polytechnique de Montréal.

[6]. Johnson, G.R., Cook, W.H., 1983.A Constitutive Model and Data for Metals Subjected to Large Strains, High Strain Rates, and High Temperatures. Proceedings 7th International Symposium on Ballistics, The Hague, 19-21 April 1983, pp541-547.

[7]. Ali, D.K., Serradj, N.B. and Ghernaout, M.E.A., 2018. 'Qualification and Validation of an in-situ Measurement Method of the Machining Temperature,' in Mechanisms and machine science, pp. 15–27. https://doi.org/10.1007/978-3-319-89911-4_2.

[8]. Akhil, C.S., Ananthavishnu, M.H., Akhil, C.K., Afeez, P.M., Akhilesh, R. and Rahul, R., 2016. Measurement of cutting temperature during machining. IOSR Journal of Mechanical and Civil Engineering, 13(2), pp.108-122.

[9]. Komanduri, R. and Hou, Z.B., 2001. A review of the experimental techniques for the measurement of heat and temperatures generated in some manufacturing processes and tribology. Tribology international, 34(10), pp.653-682.

[10]. Conradie, P.J.T., Oosthuizen, G.A., Treurnicht, N.F. and Al Shaalane, A., 2012. Overview of work piece temperature measurement techniques for machining of Ti6Al4V. South African Journal of Industrial Engineering, 23(2), pp.116-130.

[11]. Da Silva, M.B. & Wallbank, J. 1999. Cutting temperature: Prediction and measurement methods -a review, Journal of Materials Processing Technology, 195-202.

[12]. Davies, M.A., Ueda, T., M'Saoubi, R. Mullany, B. & Cooke, A.L. 2007. On the measurement of temperature in material removal processes, Annals of the CIRP, Vol.56, No.2, 581-604.

[13]. Longbottom, J.M. & Lanham, J.D. 2005. Cutting temperature measurement while machining - A review, Aircraft Engineering and Aerospace Technology, pp.122-130.

[14]. Sutter, G., Faure, L., Molinari, A., Ranc, N. & Pina, V. 2003. An experimental technique for the measurement of temperature fields for the orthogonal cutting in high speed machining, International Journal of Machine Tools & Manufacture, 671-678.

[15]. O'Sullivan, D. & Cotterell, M. 2001. Temperature measurement in single point turning, Journal of Materials Processing Technology, 301-308.

[16]. Yang, J., Sun, S., Brandt, M. & Yan, W. 2010. Experimental investigation and 3D finite element prediction of the heat affected zone during laser assisted machining of Ti6Al4V alloy, Journal of Materials Processing Technology, 210 (1), 2215–2222.

[17]. Cengel, Y.A. 2006. Heat and mass transfer. New York: McGraw-Hill.

[18]. Sales, W.F., Guimaraes, G., Machado, A.R. & Ezugwu, E.O. 2002. Cooling ability of cutting fluids and measurement of the chip-tool interface temperatures, Industrial Lubrication and Tribology, pp.57-68.

[19]. Potdar, Y.K. & Zehnder, A.T. 2004. Temperature and deformation measurements in transient metal cutting, Society for Experimental Mechanics, pp.1-9

[20]. Longbottom, J.M. & Lanham, J.D. 2005. Cutting temperature measurement while machining - A review, Aircraft Engineering and Aerospace Technology, pp.122-130.

[21]. Multi-Wavelength Ultra-Weak Fibre Bragg Grating Arrays for Long-Distance Quasi-Distributed Sensing

[22]. Leonidas, E., Ayvar-Soberanis, S., Laalej, H., Fitzpatrick, S. and Willmott, J.R., 2022. A comparative review of thermocouple and infrared radiation temperature measurement methods during the machining of metals. Sensors, 22(13), p.4693.

[23]. Davies, M.A.; Ueda, T.; M'Saoubi, R.; Mullany, B.; Cooke, A.L. On The Measurement of Temperature in Material Removal Processes. CIRP Ann.-Manuf. Technol. 2007, 56, 581–604. [CrossRef]

[24]. Saunders, P. Fundametals of Radiation Thermometry; SPIE Press: Bellingham, WA, USA, 2007.

[25]. Cotterell, M.; Ares, E.; Yanes, J.; López, F.; Hernandez, P.; Peláez, G. Temperature and strain measurement during chip formation in orthogonal cutting conditions applied to Ti-6Al-4V. In Proceedings of the Procedia Engineering, Zaragoza, Spain, 26–28 June 2013; Elsevier Ltd.: Amsterdam, The Netherlands, 2013; Volume 63, pp. 922–930. [CrossRef]

[26]. Vollmer, M. and Möllmann, K.-P. (2018) Infrared thermal imaging: Fundamentals, Research and Applications. John Wiley & Sons.

[27]. rra-Castanedo, C. and Maldague, X.P., 2013. Infrared thermography. In Handbook of Technical Diagnostics: Fundamentals and Application to Structures and Systems (pp. 175-220). Berlin, Heidelberg: Springer Berlin Heidelberg.

[28]. racovschi, E., 2014. Vitrocéramiques infrarouges pour application à la vision nocturne (Doctoral dissertation, Rennes 1).

[29]. Musikant, S. 2003. Glass. In Encyclopedia of Physical Science and Technology. 3rd ed. Academic press.

[30]. Hou, F., Zhang, Y., Zhou, Y., Zhang, M., Lv, B. and Wu, J., 2022. Review on infrared imaging technology. Sustainability, 14(18), p.11161.

[31]. Swamidoss, I.N., Amro, A.B. and Sayadi, S., 2021. Systematic approach for thermal imaging camera calibration for machine vision applications. Optik, 247, p.168039.

[32]. ElSheikh, A., Abu-Nabah, B.A., Hamdan, M.O. and Tian, G.Y., 2023. Infrared camera geometric calibration: a review and a precise thermal radiation checkerboard target. Sensors, 23(7), p.3479.

[33]. Leonidas, E., Ayvar-Soberanis, S., Laalej, H., Fitzpatrick, S. and Willmott, J.R., 2022. A comparative review of thermocouple and infrared radiation temperature measurement methods during the machining of metals. Sensors, 22(13), p.4693.

[34]. Rahman, M., Senthil, K.A. & Choudhury, M.R. 2000. Identification of effective zones for high pressure coolant in milling, Annals of the CIRP, 47-52.

[35]. Longbottom, J.M. and Lanham, J.D., 2005. Cutting temperature measurement while machining–a review. Aircraft Engineering and Aerospace Technology, 77(2), pp.122-130.

[36]. *"Mini infrared thermometer: Fluke 62 Max ir thermometer" Fluke*, https://www.fluke.com/en-us/product/temperature-measurement/ir-thermometers/fluke-62-max. Accessed 12 June 2024.

[37]. "IR spectroscopy review: Organic Chemistry Help" Organic Chemistry Help | Master Organic Chemistry With Our Proven Method, https://www.studyorgo.com/blog/ir-spectroscopy-review/. Accessed 12 June 2024.

[38]. "Thermographie Infrarouge." THERMOCONCEPT, www.thermoconcept-sarl.com/documents/thermographie-infrarouge/. Accessed 21 Mar. 2024.

[39]. Nedić, B., 1991. Upravljanje procesom obrade otvora bušenjem. Magistarski rad, Mašinski fakultet, Kragujevac.

[40]. Johnson, G.R., Hoegfeldt, J.M., Lindholm, U.S. and Nagy, A., 1983. Response of various metals to large torsional strains over a large range of strain rates—Part 1: Ductile metals.

[41]. Serradj, N.B., Ali, A.D.K. and Ghernaout, M.E.A., 2021. A Contribution to the Thermal Field Evaluation at the Tool-Part Interface for the Optimization of Machining Conditions. Engineering, Technology & Applied Science Research, 11(6), pp.7750-7756.

[42]. “Flir SC-305 SC-325 SC-645 SC-655 High Resolution Infrared Camera for Research & Development laboratory university medical veterinary medical academic.” Distek measurement instruments, https://www.distek.ro/en/Product/Flir-SC-305-SC-325-SC-645-SC-655-High-Resolution-Infrared-Camera-for-Research-and-Development--2060. Accessed 14 Jun. 2024.